LOW-COST, LOW INFRASTRUCTURE X-BAND DOPPLER RADAR DEVELOPMENT

by

Wilson Castellano

A project report submitted in partial fulfillment of the requirements for the degree of

MASTER OF ENGINEERING
in
ELECTRICAL ENGINEERING

UNIVERSITY OF PUERTO RICO
MAYAGÜEZ CAMPUS
2011

Approved by:

______________________________ __________________
José G. Colom Ustáriz, PhD Date
Member, Graduate Committee

______________________________ __________________
Rafael A. Rodríguez Solís, PhD Date
Member, Graduate Committee

______________________________ __________________
Sandra L. Cruz-Pol, PhD Date
President, Graduate Committee

______________________________ __________________
Uroyoán R. Walker Ramos, PhD Date
Representative of Graduate Studies

______________________________ __________________
Pedro Rivera, PhD Date
Chairperson of the Department

ABSTRACT

The Student Led Test Bed (STB) is part of the NSF Engineering Research Center CASA and is focused on developing and deploying low cost and low infrastructure weather radars to fill lower atmosphere gaps not covered by current technology. In fact, some of these radars are deployed in western Puerto Rico where precipitation measurements are made to complement measurements taken with the NWS NEXRAD radar. These radars have the option of using solar power and thus can be independent of the power grid, so they are known as Off-The-Grid (OTG) X-band radars. However; they are only capable of providing rain reflectivity measurements. A modification was performed to achieve Doppler capabilities for this radar so they can also measure wind speed. This enhancement was conducted because Doppler capabilities allow the use of superior clutter removal algorithms than those used for reflectivity-only radars, and the radar provides additional information about low level winds in weather events in western Puerto Rico.

This project report describes the initial work in the development of the first OTG X-band Doppler radar based on modifications of a marine radar. Two methods to develop a coherent radar are discussed, the Injection Frequency Lock (IFL) method and the Pseudo Coherent method. From these two methods, the Pseudo coherent method was selected after some tests performed at the Microwave Remote Sensing Laboratory (MIRSL) at the University of Massachusetts. As a result a more detailed description of this method is presented in this project report.

RESUMEN

El lugar de prueba liderado por estudiantes (STB por sus siglas en inglés) es parte del Centro de investigación de ingeniería de la Fundación Nacional de Ciencia (NSF por sus siglas en inglés) llamado CASA y se enfoca en el desarrollo, ensamblaje e instalación de radares meteorológicos de bajo costo y baja infraestructura para cubrir los espacios en la atmósfera baja que no son cubiertos por la tecnología actual. De hecho, algunos de estos radares están instalados en varias localizaciones de la región oeste de Puerto Rico, donde se toman medidas de precipitación para complementar las medidas tomadas por el radar NEXRAD del Servicio Nacional de Meteorología (NWS). Estos radares tienen la opción de operar independientemente de la red eléctrica, por lo que se conocen como OTG (por sus siglas en inglés) y transmiten en banda X. Sin embargo, sólo son capaces de proporcionar medidas de reflectividad de lluvia. Por lo tanto, algunas modificaciones se llevaron a cabo para lograr obtener medidas Doppler para obtener velocidad de viento. Estas modificaciones se llevaron a cabo debido a que la data Doppler permite el uso de algoritmos superiores para la eliminación de reflecciones capturadas que no son deseadas y el radar proporciona información adicional acerca de los vientos de velocidad baja de los fenómenos meteorológicos en el oeste de Puerto Rico.

Este reporte de proyecto describe el trabajo inicial en el desarrollo del primer radar Doppler de banda X OTG a partir de modificaciones hechas a un radar marino comercial. Dos métodos para desarrollar un radar coherente son discutidos, un método está relacionado con la inyección de una señal para amarrar la frecuencia del magnetrón del radar a la frecuencia de la señal inyectada (IFL por sus siglas en inglés) y el otro método se conoce como seudo coherente. De estos dos métodos, el método seudo coherente fue seleccionado después de algunas pruebas realizadas en el Laboratorio de Percepción Remota por Microondas (MIRSL, por sus siglas en inglés) de la Universidad de Massachusetts. Como resultado, una descripción detallada de este método es presentado en este reporte de proyecto.

To my family and fiancée…

He who walks with the wise grows wise…

-Proverbs 13:20

ACKNOWLEDGMENT

First, I would like to thank God for giving me both, the opportunity to breathe each day and His blessings through my years of study. I also thank my family for their support and my fiancée Zulmarie Jiménez for being at my side with words of encouragement and motivation. I also acknowledge my advisor Sandra Cruz Pol and the members of my committee, José Colom Ustáriz and Rafael Rodriguez Solis, for the opportunity of doing research with them and for the time they spent supporting and guiding me during my research.

I would like to thank the people from the Cloud Microwave Measurements of Atmospheric Events (CLiMMATE) Laboratory at the University of Puerto Rico at Mayagüez for the work done and each moment we spent together. Thanks for your support and friendship: José Rosario “Joito”, Benjamín De Jesús “Pito”, José Ortiz “Kotshie”, José Cordero, Estefany Lancheros, Keyla Mora, Luz Torres and thanks to those already gone from the lab for your support as well during your studies at UPRM: María Fernanda Cordoba Erazo, Gianni Pablos and Melissa Acosta. I also want to acknowledge professor Leyda León for her help.

I want to mention people from UMASS as well which were very helpful during the summer I spent at the Microwave Remote Sensing Laboratory (MIRSL). I would like to start giving thanks to CASA’s Director of Education and Outreach, Dr. Paula Sturdevant Rees who arranged all the paper work at UMASS for my stay. Also, I give thanks to Eric Knapp, who took some time to share his vast experience in radars and guided me through the research. Professor Stephen Frasier was also a big help because of his previous experiences with radar components. Also, I want to express deep and sincere gratitude to Jorge Trabal, Rafael Medina and Jorge Salazar who made my stay at Amherst a pleasant one. Thanks for sharing with me many moments that I will certainly remember the rest of my life.

Finally, I want to be grateful to the ECE department professional counselor, Madeline Rodríguez, who allowed me to develop my leadership skills during my undergrad and graduate years while working with her. It always makes me happy to find kind and friendly people like her on my way. Also, I like to thank the UPRM R&D staff, Carlos Mercado and his crew and the graduate academic counselor Sandra Montalvo. These people help me solved issues indirectly related with my research and graduate studies. The Grant from NSF 0313747 provided the funding and the resources necessary for this research development.

Table of Contents

Table List

Figures List

1. Introduction

1.1 Motivation

The National Weather Service (NWS) office in San Juan provides weather information using the NEXRAD radar technology deployed at Cayey. The radar at Cayey presents some limitations while detecting weather events in western Puerto Rico. These limitations are caused because the earth's curvature prevents the lower boundary layer from being observed at distances far from the radar, missing a significant amount of information [*Skolnik*, 1980]. The Engineering Research Center (ERC) for the Collaborative Adaptive Sensing of the Atmosphere (CASA) has developed a new approach to obtain better atmospheric data from weather events [*McLaughlin et al*, 2009]. This new paradigm consist of a network of small radars and is used to cover the gaps in the lower atmosphere not covered by the current NEXRAD radars, including the one at Cayey, Puerto Rico. The Student Test Bed (STB) implemented a radar network in the western region using modified X-Band FURUNO® marine radars [*Pablos*, 2010] [*Trabal et al.,* 2011]. These modified marine radars are capable of obtaining rain reflectivity measurements with the modifications made. Some modifications include mounting a parabolic reflector antenna instead of the fan beam antenna normally used for marine applications, among others in the control and data acquisition system. Other work was performed to mitigate the clutter problem using data processing algorithms [*Acosta*, 2011].

This low-cost, low-infrastructure X-Band FURUNO® marine radar will be modified to have Doppler capabilities which is the topic of this project report, and will continue to be used for weather applications. It is one of a kind because there are no OTG (Off-The-Grid) Doppler radars available in the market yet. This enhancement was done because the Doppler capabilities allow the use of superior clutter removal algorithms than those used for reflectivity-only radars, and the radar provides additional information about weather events such as wind speed.

The principal motivation of this research was to study methods of adding the Doppler capabilities maintaining the radar as simple as possible while keeping the manufacturing cost low. One of the methods considered was a circuit that allows the injection of a signal to achieve the frequency lock of the magnetron resulting in a coherent radar. According to *DeVito et al.* [1967], coherent radar employing an injection-locked magnetron could improve the range-resolution, reduce the clutter and decrease the radar's vulnerability to jamming. The other method is known as pseudo coherent radar or coherent on receive and consist of having coherence between the transmitted frequency and the receiver reference signal [*Junyent*, 2007]. These two signals are compared and the Doppler data is obtained as the result of the comparison.

1.2 Objectives

The goal of this research was to design the necessary modifications for a FURUNO® marine radar in order to increase its capabilities as a Doppler weather radar. This radar is one of a kind because Doppler radars are big and expensive and this one was developed from a modified marine radar. In most cases, radar engineers design and build radars from scratch; but, in this case, modifications were done to commercially available marine radars in order keep costs low. This brought new challenges to the design because of the required compatibility of new equipment and the circuits already installed in the radar. The space available inside the marine radar to place new circuits was another limitation.

As a second goal, this research solved challenges in order to achieve accurate Doppler data. Some of these challenges are due to the fact that commercially available marine radar was used. The challenges included the revolution-per-minute (RPM) reduction in order to properly distinguish stationary objects from the ones moving. Another challenge is increasing the pulse repetition frequency (PRF), which solves ambiguity problem or aliasing in the echoes received. In addition, feedback loop circuit was implemented to correct the frequency drift in the magnetron caused by the changes in temperature.

Finally, the acquisition of a different data acquisition card (DAQ card) required some programming to correctly process the data obtained.

1.3 Literature Review

Since their invention, radars have been improved to increase their sensing capabilities [*Pablos*, 2010]. Today, radars are used by the military and commercial agencies to obtain information according to human kind's needs. Radars have been deployed in land, sea and air platforms; but for weather applications, ground-based radars are common. Ground-based radars are mostly installed in high mountains to obtain an obstruction-free beam angle view in tracking and targeting applications [*Trabal*, 2003]. Examples of ground-based radar are meteorological radars.

These radars are typically deployed at high mountains as well. This causes loss of important information of the lower troposphere (1-2 Km), where most weather phenomena occurs, due to the Earth's curvature as the beam of the radar gets further away [*Trabal*, 2011]. The diagram in Figure 1.1 provides a better understanding of this problem.

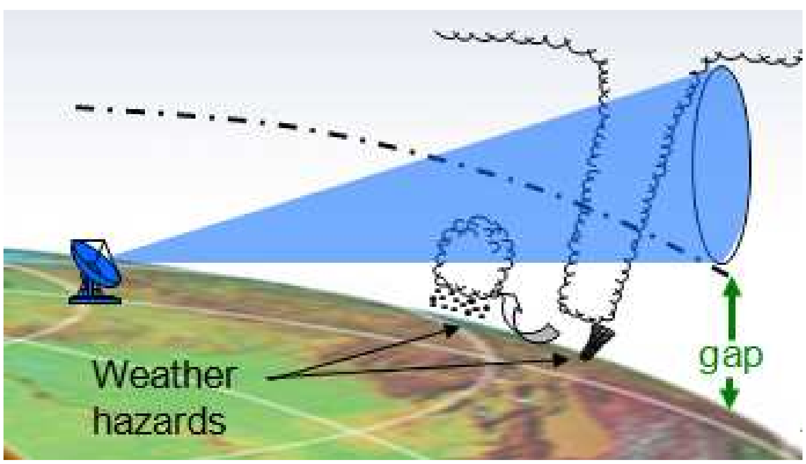

Figure 1.1 Earth's curvature effect

Figure 1.1 represents the sensing gap problem that CASA intends to solve with short-range weather radars. This sensing gap of the lowest troposphere becomes worst in countries with complex topographies, like Puerto Rico. That is why long-range radars are not an optimum solution to monitor the lower troposphere in that situation [*Acosta,* 2011].

The NWS Weather Forecast Office at San Juan, PR uses the TJUA radar (NEXRAD WSR-88D technology) deployed at Cayey to monitor weather events. Meteorologists use this radar data and products to make weather predictions and issue any necessary warning message in the island. This radar is mounted at a height of 881m above sea level and more than a 100 km southeast from western Puerto Rico, where Mayagüez is located [*Trabal et al.,* 2011]. Because of the distance and the beam blockage due to the central mountains in PR, the TJUA radar fails to capture accurate weather information in western Puerto Rico. That problem is the motivation behind the CASA research group deployment of a low-cost and low infrastructure radar network using modified marine radars improving the spatial and temporal resolution of weather observations, and providing gap coverage of the lower atmosphere not covered by NEXRAD [*Acosta et al.,* 2011]. The radars operate at the X-band frequency use a magnetron power source to transmit the trend of pulses in a single polarized mode. Further specifications about the OTG FURUNO® marine radar is found in section 2.2.7.

Figure 1.2 shows the location of the network of three radars and their coverage area. The triangular configuration was selescted to maximize the overlap coverage between the radars as shown in the figure. The figure also provides an example of the data that can be collected by these radars. The data image represents the reflectivity obtained after processing and merging data from the radars. The equation used to obtain the reflectivity can be described as follows [*Skolnik*, 1980]:

$$\overline{P_{cal}} = \frac{P_t G_{ant}^2 \lambda^2 G_s \sigma_{cal}}{10^3 (4\pi)^3 L_{tx} l_r l_{ac}^2 R_{cal}^4} \ [mW] \tag{1.1}$$

where P_{cal} is the calibrated measured power, P_t is the transmitted power, G_{ant} is the antenna gain, λ is the wavelength of the electromagnetic wave transmitted by the radar, G_s is the system gain, σ_{cal} is the radar cross section of the known target, L_{tx} is the transmission loss, l_r is the receiver loss, l_{ac} is the loss of the path, and R_{cal} is the distance or range at which the measurement was collected.

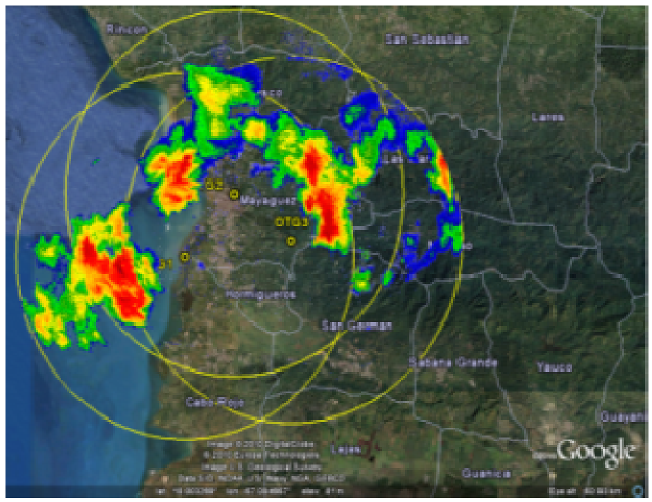

Figure 1.2 Map and sample of collected data overlaid Google terrain maps

Some modifications can increase these radar's capabilities to develop a coherent radar. Coherence is obtained when the phase of the transmitted pulse is known and conserved to process the received signal. The most important ability of a coherent system is its ability to discern small differences in Doppler velocity changes. These differences in velocity correspond to small differences in phase. The coherent processing offers Doppler resolution/estimation and provides less interference and signal/noise benefits relative to non-coherent processing [*Wolff*, 1997].

The use of the Doppler effect improves the probability of detection and the measurement accuracy [*Richards*, 2010]. Doppler effect is the change in frequency when a radiation source moves radially either away or toward a target or when the target is moving and the radiation source is stationary.

A good example is an ambulance when it has its siren on and drives through a street filled with people. They can hear the change in sound frequency as the siren moves closer or away from the observer. In the case of radars, the radar is stationary but observing moving targets [*Rinehart*, 2010]. Each target will shift the frequency of the radar signal depending on its speed. The phase of an electromagnetic wave is the fraction of a full wavelength [*Richards*, 2010]. A phase shift can be either positive or negative with respect of a reference point. Using a sine wave as an example, its reference point is when the sine is zero. Figure 1.3 shows two sine waves out of phase by 45 degrees.

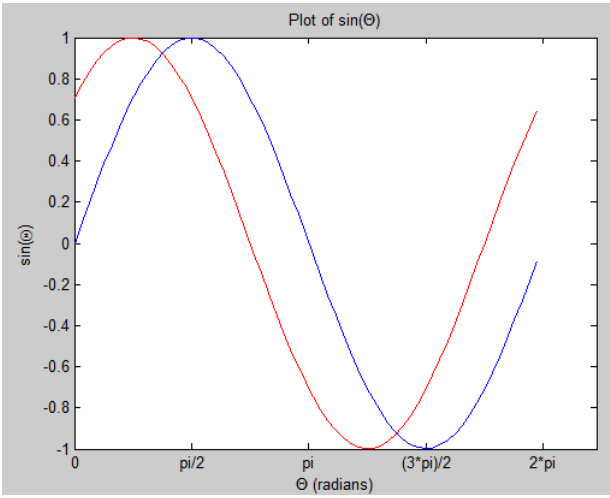

Figure 1.3 Sine waves 45° out of phase

One method to achieve coherence is by using the Injection Frequency Lock method (IFL). According to *Tahir* [2006], this concept was introduced in early 50's and consists of creating a low power signal with a stable oscillator and injecting this signal, with distinctive phase characteristics, into the interaction circuit of the magnetron. If the frequency of the magnetron and the frequency of the oscillator are sufficiently close, the high power signal will synchronize with the injected signal and a single frequency output will be achieved [*De Vito et al.*, 1969]. Then, the magnetron will transmit a pulse with similar phase pattern as the oscillator. Figure 1.4 shows this concept graphically.

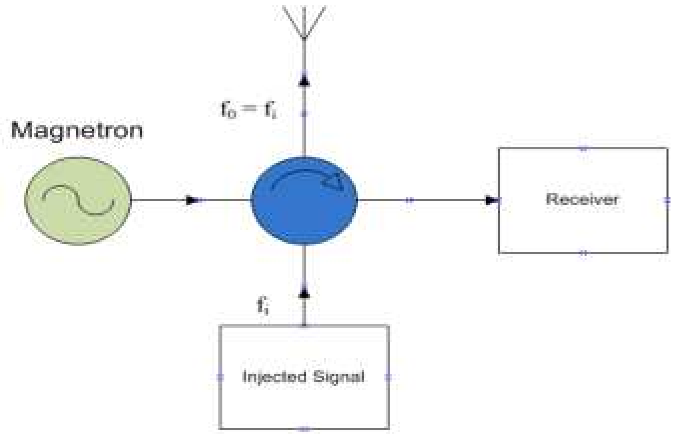

Figure 1.4 Injection Frequency Lock Method

Another method is by developing a pseudo coherent radar receiver. This method implies major changes to the receiver in order to record the phase of the transmitted signal and obtain the in-phase and quadrature phase (I and Q) signals from the received echo. It also requires a stable continuous-wave (CW) reference oscillator signal, which is locked in phase with the transmitter during each transmitted pulse and is mixed with the echo signal to produce a difference signal. Since the reference oscillator and the transmitter are locked in phase, the echoes are effectively compared with the transmitter in frequency and phase. This phase reference must be maintained from the transmitted pulse to the return pulse picked up by the receiver.

These phase changes are calculated by monitoring the real and imaginary components of the electromagnetic signal. These components are referred as the I and Q components of a signal. The I/Q data shows the changes in magnitude and phase of a sine wave [*National Instruments*, 2011]. It is difficult to manipulate the sine wave directly using electronic components and it could be very expensive; but controlling the sine wave components is easier. There are many electronic components commercially available to read and manipulate the sine wave components known as the I and Q signals. These components are demodulators and modulators. Figure 1.5 shows a traveling signal (green) and it's I and Q components (red). These components are, basically, a projection to the green signal and contain information related to the traveling signal's phase.

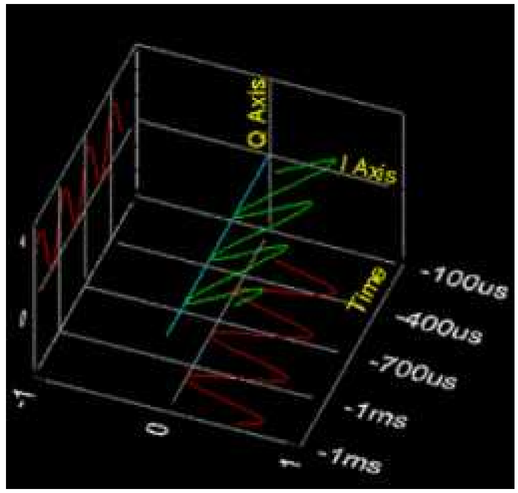

Figure 1.5 I and Q signals projection from a traveling wave [*National Instruments*, 2011]
http://zone.ni.com/devzone/cda/tut/p/id/4805

1.4 Summary of chapters

The first chapter comprises the background information of this research. It presents the motivations and the objectives of this research work. The second chapter presents the background theory. In this section a brief history of radars is discussed. In addition, the Doppler radar parameters and related topics are discussed to have a better understanding of the Doppler velocity measurements. The third chapter is devoted to the explanation of the Injection Frequency Locked (IFL) method. This section includes the description of the necessary materials, including cost, to lock the magnetron's frequency to another signal's frequency. In addition, the section describes the bench tests that were conducted and their results. The fourth chapter describes the pseudo-coherent or coherent on receive methods. It contains a description of the necessary materials and their cost as in section three. Moreover, it obtains the description of the tests that were performed and their results. Chapter five presents the challenges and solutions for the problems mentioned in the objectives. The data collected by the modified marine radar is presented and explained in chapter six, including the description of the tests conducted. The conclusions and the future work form part of chapter seven.

2. Background Theory and Specifications

2.1 History

The history of radars is closely related to the history of radios. In fact, the word radar is an acronym that stands for *"radio detection and ranging"*. Thinking in the history of radars means keeping in mind the discoveries made in 18th, 19th and early 20th centuries that showed the way for the use of radios as communication devices [*Rinehart*, 2010].

The radars function is directly related to the properties of an electromagnetic wave as it interacts with a physical object [*Peebles*, 1998]. Thus, the earliest roots of radar can be related to the work done by James Clerk Maxwell in 1865 when he predicted electromagnetic waves propagation [*Peebles*, 1998], and with the invention of radio (transmission) by Nikola Tesla [*Cheney*, 1981]. This work was verified by Heinrich Rudolf Hertz in 1886. Hertz's experimental work showed that an electromagnetic wave could be reflected by physical objects. His work represents what radars do; they detect the presence of a reflected wave to determine the existence of targets [*Peebles*, 1998]. But it was Hulsmeyer in the early 1900s who developed something similar to a monostatic pulse radar. He got a patent from England and other countries and tried to sell his invention to ship owners, but no one showed interest at the time [*Skolnik,* 1980].

In the 1920s evidence of radar method appeared. Taylor and Young were able to detect disturbance in their receiver when a ship passed between their transmitter and receiver at Potomac River. In addition, Breit and Tuve used a radar, not recognized at the time, to measure the height of the ionosphere. Some other reported detection were made using a system similar to a bistatic radar, but the appearance of heavy military bomber aircraft in the late 1920s and 1930s that gave rise to operational military radars [*Skolnik*, 1980].

After World War I, the bomber was modified and the need of detecting this aircraft increased. In many countries the development of an instrument to detect bombers was similar even though they were a secret. Many technologies were examined: sound locators, infrared and bistatic radars, but none were successful. Some didn't cover an extensive range and others acted as a trip wire to detect passing objects. The radar method did not become useful until the transmitter and receiver were collocated at a single site and pulsed waveforms were used [*Skolnik,* 1980].

Basically, radars were rediscovered and developed almost simultaneously in the United States, United Kingdom, Germany, Soviet Union, France, Italy, Japan and Netherlands. These radars operated in frequencies significantly lower than current technology. Comparing with microwave radars, they had some limitations, but they did their intended job [*Skolnik,* 1980].

Today improvements have been made in various radar components like transmitters, receivers, displays, processors, antennas and the application of computers to radars. In fact, the software of a radar is as important as the hardware because it makes possible providing automatic warnings only by processing radar data with computers. Once of the greatest achievements in radars was the development of Doppler techniques. Doppler radars provide measurements of power received from a target and its radial velocity which is useful in surveillance applications.

2.2 Doppler Radar Parameters

This section presents the definition and examples of various important parameters used during the research. These parameters were helpful to understand the functionality of a Doppler radar and to identify problems in the system and their solution.

2.2.1 Doppler

Any apparent change in frequency of an electromagnetic (EM) wave is known as the Doppler effect. This change in frequency is detected by observing the phase of an EM wave which is a fraction of the full wave. The total phase change is calculated with the range to target *r* and the wavelength λ with the following equation:

$$\phi = \frac{4\pi r}{\lambda} \tag{2.1}$$

By differentiating the equation above with respect to time gives the rate of change of phase, which is the angular frequency

$$\omega_d = \frac{4\pi}{\lambda}\frac{dr}{dt} = \frac{4\pi v_r}{\lambda} = 2\pi f_d \tag{2.2}$$

where v_r is the radial velocity and f_d is the Doppler frequency shift. Rearranging equation (2-2), equation (2.3) is obtained.

$$f_d = \frac{2v_r}{\lambda} \tag{2.3}$$

Notice that it is linearly proportional to the velocity and inversely proportional to wavelength; which is constant for given radar. Thus, the frequency shift depends only of the velocity of the target; but if the target is not moving directly toward or away from the radar, equation (2.3) needs to be corrected to add the radial component of motion.

$$f_d = \frac{2Vcos(\alpha)}{\lambda} \tag{2.4}$$

where α is the angle formed between the velocity vector of the target and the beam. This concept is illustrated with figure 2.1.

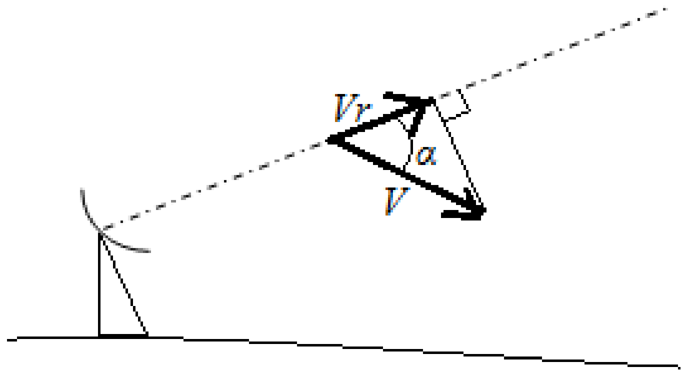

Figure 2.1 Radial motion of a target

A pulse radar, depicted in figure 2.2, is commonly used to obtain Doppler frequency-shifted echo signal. This is achieved when the output of a stable oscillator is amplified by a high-power amplifier. The amplifier is modulated to generate high-power pulses. The received echo signal is mixed with the stable oscillator output to recognize any changes in the received echo-signal frequency. Then, the frequency shift is detected by the Doppler filter and the velocity of the received signal is derived.

$$V_{rec} = A_r \sin\left[2\pi f_t\left(1+\frac{2v_r}{c}\right)t - \frac{2\pi f_t R_0}{c}\right] \tag{2.5}$$

Due to the changes in the received frequency by a factor of $2f_t v_r/c = 2v_r/\lambda = f_d$ and the mixing of the received signal with the reference signal, equation (2.5) becomes,

$$V_d = A_d \cos\left[2\pi f_d t - \frac{4\pi R_0}{\lambda}\right] \tag{2.6}$$

where A_d is the amplitude, f_d is the Doppler frequency and R_0 is the initial range of a detected moving target.

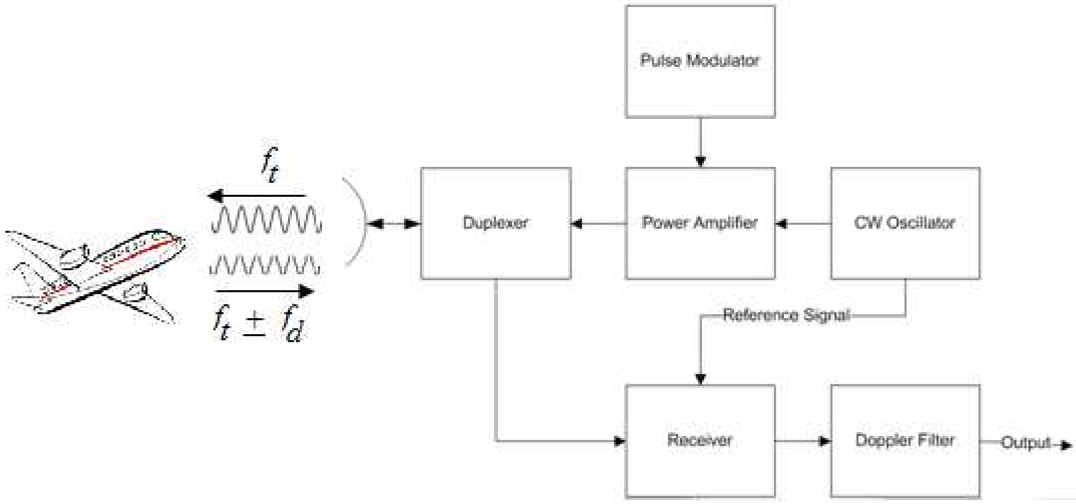

Figure 2.2 Block diagram of simple pulse radar detecting a moving target

2.2.2 Pulse Waveform

Pulse radars transmit EM waves during a small period of time. This time duration is known as the *pulse width* τ and during this time the receiver is isolated from the antenna to protect its sensitive components from the high power pulse. No received signal can be detected at this time. Then, after the pulse is transmitted the receiver connects to the antenna to listen echoes from the reflected signal. This listening time plus the pulse width is known as the *pulse repetition interval (PRI)*, which is inversely proportional to the *pulse repetition frequency (PRF)*. The PRF is the number of transmit/receive cycles in radar. In addition, the duration of the transmission period is called the *duty cycle* (d_t), which is given by the following relation,

$$d_t = \frac{\tau}{PRI} = \tau \cdot PRF \tag{2.7}$$

Most of these concepts are represented in figure 2.3 below.

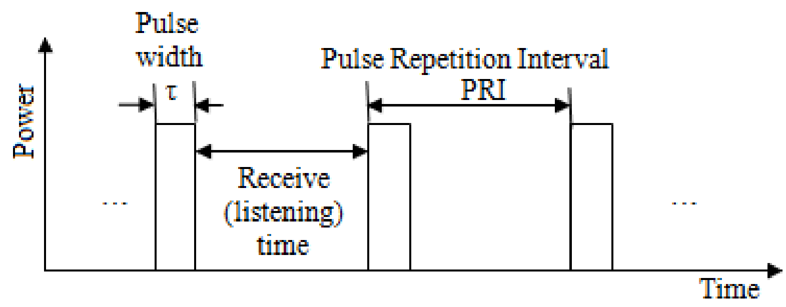

Figure 2.3 Pulse waveforms concepts example

2.2.3 Unambiguous Range

When radars transmit a pulse they cannot wait forever to send the following pulses. In real world, the next pulse goes out when the PRI is completed. This is done because radars cannot detect targets at a very long ranges, the echo is too weak to be detected. In the given case when an EM wave does not return to the radar's receiver before the next pulse is transmitted, this results in a time ambiguity and associated range ambiguity. This means that the received echo could be from the pulse that was just transmitted which means a close-in target or it could be from the pulse previously transmitted, a distant target. This can cause a big problem while analyzing the data; but, fortunately, it can be avoided.

To avoid this issue the PRF should be low enough, such that echoes of interest reach the receiver before the second pulse is transmitted. It is known that the round-trip time for the radar wave is,

$$\Delta T = \frac{2R}{c} \tag{2.8}$$

And from here the following condition must be satisfied to prevent range ambiguities:

$$PRI \geq \Delta T_{max} = \frac{2R_{max}}{c} \quad or \quad R_{max} \leq \frac{c \cdot PRI}{2} = \frac{c}{2PRF} \tag{2.9}$$

where R_{max} is the maximum target range of interest. Thus, the unambiguous range is the maximum range measured unambiguously by the radar and given by

$$R_{ua} = \frac{c}{2PRF} \tag{2.10}$$

2.2.4 Unambiguous Velocity

There are limitations as well in the velocities that a radar can resolve unambiguously. When a target is not moving toward or away the radar it will have zero radial velocity; but this doesn't means that the target is stationary. This happens if the target remains at a constant distance from the radar or if it moves orthogonally to the radar's beam.

The maximum velocity a Doppler radar can detect is given by the velocity which produces a phase shift of $\pm\pi$ radians. This is called Nyquist velocity and it is represented mathematically as

$$V_{max} = \frac{\pm f_{max}\lambda}{2} \tag{2.11}$$

where the maximum frequency is given by

$$f_{max} = \frac{PRF}{2} \tag{2.12}$$

and PRF is the pulse repetition frequency. Thus the maximum unambiguous velocity detectable by a Doppler radar is

$$V_{max} = \frac{\pm PRF\lambda}{4} \tag{2.13}$$

2.2.5 Doppler Dilemma

Maximizing unambiguous range leads to lower PRFs (see eq. 2.10) and maximizing unambiguous velocity leads to higher PRFs (see eq. 2.13). In many systems, no single PRF can meet both opposing requirements. This problem is commonly known as the "Doppler dilemma". By solving both equations and equating them it is found that

$$V_{max}R_{max} = \frac{c\lambda}{8} \tag{2.14}$$

It can be seen from equation 2.14 that a tradeoff between velocity and range needs to be made. To solve the Doppler dilemma one particular solution can be applied, selecting longer wavelength. This means that the radar can be lower in frequency, bigger and more expensive. In this project in particular (CASA) this change is not applied to keep the high resolution obtained with the radars and the costs low.

2.3 OTG System Specifications

The transmitted pulses from the FURUNO® radar are generated with a magnetron oscillator. These waves fit the WR-90 waveguide used through the X-Band system. The following table shows important specifications of the magnetron.

Table 2.1 Magnetron parameters

Frequency	9410 ± 30 MHz
Heater Voltage	6.3 V
Heater Current	0.55 A
Cathode warm-up time	90 s
Pulse Width	0.05 – 1.1 μs
Duty	0.001
Load VSWR	1.5
Peak output power	4 kW

In addition, there are some system parameters of the FURUNO® radars. These parameters are presented below.

Table 2.2: System Parameters

Operational Range	15.36 km
Rated Voltage	12 – 24 V
Rated Current	5.6 – 2.7 A
Frequency	9410 ± 30 MHz
Wavelength	0.03188 m
Peak Power	4 kW
Intermediate frequency	60 MHz
Pulse length	0.8 μs
PRF	600 Hz
Bandwidth	3 MHz
Minimum Detectable Signal	-105 dBm
Noise figure	4.6 dB
RPM	26
Polarization	Vertical

The antenna of the system is one of the previous modifications done to this radar. The specifications of the antenna currently used for this system are described below.

Table 2.3: Antenna parameters

Gain	32.4 dB
Beamwidth	3.8 degrees
Side lobe level (first)	22 dB

The figures below show the actual system used by CASA's radar network installed on the west coast of the island. Figure 2.4 shows the radar node installed at Cornelia Hill and photos in Figure 2.5 shows the system on the inside.

Figure 2.4 Cornelia Hill radar node

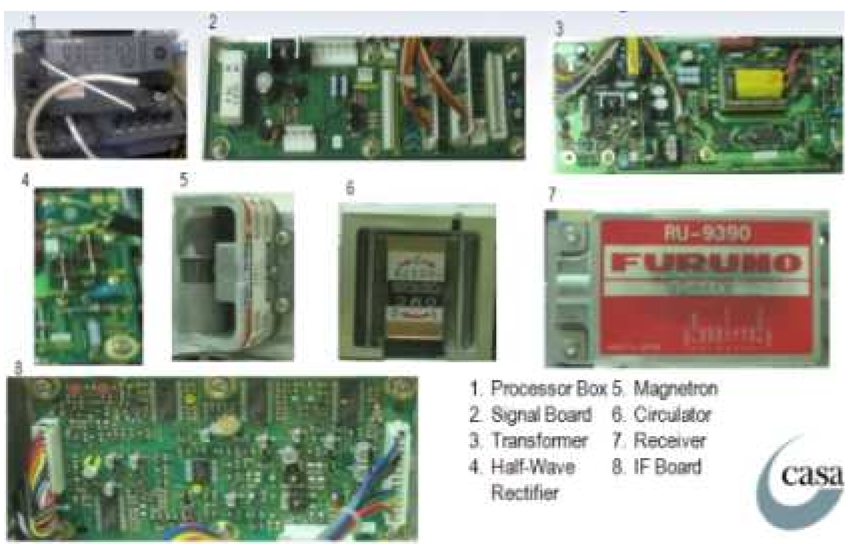

Figure 2.5 System boards and components

The operation of the radar is described as follows. The processor box communicates with the signal board, which communicates with the power supply board to transform the commands from the processor box into a power signal. This signal passes through the half-wave rectifier board and reaches the magnetron. The magnetron generates the transmitted wave, which then passes through the oscillator and exits the system at the antenna. Every echo received back at the antenna goes through the receiver; where it is digitally down converted and processed at the IF board. Then, it reaches the signal board again and goes back through the signal cable and gets to the processor box. From the processor box the data comes out; it is processed and displayed in the computer. All this process is shown in figure 2.6.

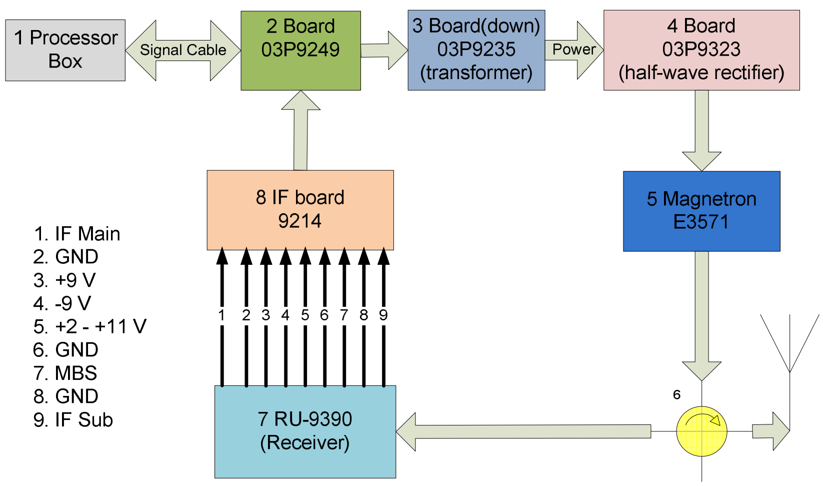

Figure 2.6 Connections on FURUNO® radar

2.4 Lab Resources

The following materials were used during characterization of materials and the tests conducted.

1. Microwave Analog Signal Generator – Was used to characterize the components and to create the signal needed for the injection-lock in early tests conducted.
2. Power Meter – Was used to characterize the components.
3. Spectrum Analyzer – Was used to verify frequency lock in the magnetron and for the characterization of the components.

4. Power Supply – Was used to power the circuits or boards added to the radar.
5. Oscilloscope – Was used to measure the IF signals.
6. Waveguide Directional Couplers – Were used to attenuate the transmitted signal before reading it with the spectrum analyzer in order to protect the ports from high power signals.
7. Coaxial Attenuators – Were used to attenuate the transmitted signal before reading it with the spectrum analyzer in order to protect the ports from high power signals.
8. Attenuators – Were used to protect equipment port from high power signals.
9. Coaxial Cables – Were used to connect everything together.
10. Waveguide to N-type connector transitions – Were used in the transitions from and to the circulators, the magnetron, the antenna port and the receiver.
11. SMA Cables – Were used to connect various components together.
12. Crocodile, Banana and Banana with Clamps Cables – Were used to power the circuits added to the radar.

3. Injection Frequency Locked Method

3.1 Method Explained

The Injection Frequency Locked (IFL) is a method where a low power signal is injected to a cavity, in this case the magnetron, to lock its high power signal's frequency to the injected signal. Figure 3.1 shows the circuit used to achieve the lock in frequency of the magnetron. This circuit was implemented between the magnetron and the circulator shown in figure 2.6 of section 2.3. As shown, a 9.41 GHz signal was generated with the Voltage Controlled Oscillator (VCO) and amplified with the HMC591LP5 X-Band High Power Amplifier. Then, this signal was inputted to the radar using the circulators to achieve the frequency lock of the magnetron. A spectrum analyzer was used to observe the frequency lock and an attenuator was placed in place to protect the instrument. The antenna of the radar was removed during the tests conducted and the spectrum analyzer was placed on its place.

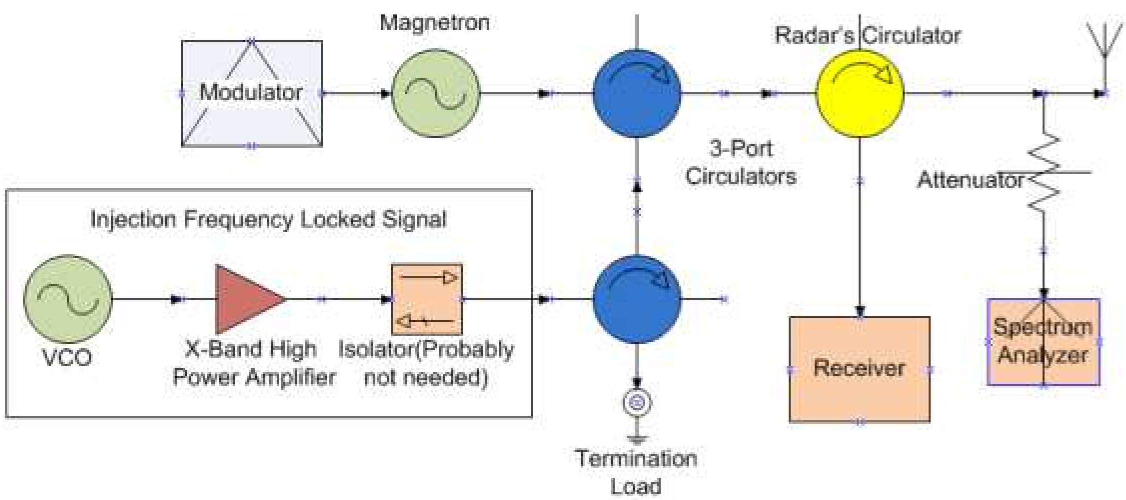

Figure 3.1 IFL Circuit Schematic

3.2 Materials

The following devices were used to achieve the IFL of the radar.

1. FURUNO® radar – Marine radar used by CASA in the Student Led Test Bed to monitor weather events.

2. X-Band Circulators – These circulators were installed in conjunction with the radar stock X-band circulator to inject the locking signal to the magnetron.
3. Signal Generator or VCO – Was used to create the low power signal injected in the magnetron to achieve the frequency lock.
4. X-Band Hi-Power Amplifier –Was used to amplify the signal generated with the VCO. This power amplifier is important in this design because the power of the signal injected from the VCO is too low and, even though, a low power signal is needed in the IFL method this signal needed to be amplified to serve its purpose.

3.3 Cost

Is part of CASA's mission to keep the cost of the project to a minimum, which makes looking at the prices of components a requirement in the design. The following table shows the preliminary cost of the radar unit with the implemented IFL modifications. Additionally, the table includes the solar power system costs and the wireless connection equipment cost. This represents the total cost of the parts in a completed OTG node of the radar network established in the island.

Table 3.1: IFL Radar Node Cost

Radar Subsystem Parts	Price
4kW FURUNO Radar	$ 7,495.00
Parabolic Antenna w/Manual adjust	$ 4,495.00
Rutter Sigma S6 Radar Processor	$ 8,300.00
Computer Hardware and Software	$ 500.00
Sub total 1	**$ 20,790.00**
Wireless Connection	**Price**
ODU External (RDW-WL 1000) (2)	$ 1,153.40
IDU-E (radio/module) (2)	$ 624.10
Antennas (24dBi, parabolic grid) (2)	$ 108.76
LMR-400 (cables) (2)	$ 33.38
Data/Signal Surge Protector (2)	$ 154.98
Lightning Arrestor (2)	$ 79.06
CAT5, 50M, RJ45 conn. (LAN cable)	$ 188.02
D-Link Switch (4 ports)	$ 40.82
Web Power Switch	$ 113.95
Sub total 4	**$ 2,496.47**

Radar Parts for Doppler capabilities	Price
X-band Circulators (2)	$ 270.00
VCO Evaluation Board	$ 397.00
Amplifier Evaluation Board	$ 518.00
Sub total 3	**$ 1,185.00**
Solar Power Sub-System	**Price**
Solar Panels (2)	$ 800.00
Batteries (2)	$ 450.00
Solar Charger	$ 200.00
Power Inverter	$ 200.00
Sub total 2	**$ 1,650.00**
Miscellaneous	**$ 500.00**

grand total	**$ 26,621.47**

3.4 Process

Once the devices and materials were received, they were individually characterized to know their behavior and performance. The circuits used depend of an input voltage to control their performance (VCO, amplifier). The characterization showed the correct tune-voltage in order to get the optimum performance of the circuits. After that, tests were conducted using the FURUNO® marine radar unit. These tests were conducted using the resources available at the lab and the frequency lock of the magnetron was achieved. All the characterization process and tests performed are described in the following sections of chapter 3.

3.4.1 VCO Characterization

The VCO was acquired as a sample from Hittite (see figure 3.2) and after powering it on, several voltages were applied at the tune-voltage pin to read the output frequency. Table 3.2 shows the readings obtained from this test.

Figure 3.2 VCO obtained

Table 3.2 VCO characterization table

Tune Voltage (V)	Frequency (GHz)
4.9	9.342
5	9.3585
5.1	9.3625
5.2	9.38
5.3	9.4087
5.4	9.425
5.5	9.44
5.6	9.4530

5.7	9.4611
5.8	9.4809
5.9	9.5017

Using 5.3V as the tune voltage gives a signal of 9.5 dBm at a frequency of 9.4087 GHz. This signal seemed adequate for the IFL; but a drift in the VCO's frequency was noted as it heated up. The need for a heat sink was shown during the characterization for one of the circuits, namely Hittite 110225, the VCO. One heat sink was put in placed in order to maintain the VCO as steady as possible.

3.4.2 2W Amplifier

The 2W power amplifier was acquired from Hittite as well as a sample. To test it, the output signal from the VCO was inputted to the circuit shown in figure 3.3.

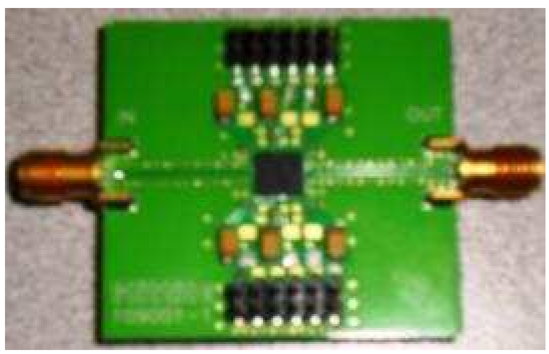

Figure 3.3 2W power amplifier

A supply voltage of 7V was applied to turn on the circuit and a reading was obtained from the output port with 18dB of gain as the datasheet stated. The signal from the VCO had a power of 9.5 dBm plus the 18 dB of gain from the amplifier meaning that the signal should have a power of 27.5 dBm. Figure 3.4 shows the reading obtained from the amplifier's output. The figure shows a signal of 22.43 dB; but it is important to mention that a 5dB attenuator was used to protect the spectrum analyzer's port. Thus, the real reading is 27.43 dBm which is in agreement to the calculations.

Figure 3.4 Two watts (2W) Amplifier Output Reading

3.4.3 Tests and Results

In addition to the characterization of the circuits used, the cables, directional couplers, connectors and transitions were characterized to take the losses into account in the measurements. All the cables had a combined loss of 0.7 dB and the connectors, couplers and transitions had a loss of 1.5 dB. Adding these losses together yields 2.2 dB in losses for these materials.

Most of the following tests were conducted at the UMASS MIRSL. The radar was set up as depicted in figure 3.5 below. Two directional couplers, one of 40 dB and the other of 20 dB, were used to protect the lab equipment from any high power signal coming from the radar. An initial measurement was made to have a reading of the transmitted power of the radar. Figure 3.6 shows that the reading was -4.6 dBm but keeping in mind that 60 dB in attenuation was introduced with the directional couplers and the cables and connectors had an additional 2.2 dB in loss the actual transmitted power of the radar is 57.6 dBm.

Figure 3.5 Radar set up at MIRSL

Figure 3.6 Power transmitted from the radar

Afterwards, the injection frequency lock was done using the 2W amplifier and the VCO with the specifications mentioned in previous sections. Every component was mounted in the radar as figure 3.1 shows in the first section of this chapter.

Figure 3.7 IFL reading with the 2W amplifier

Figure 3.7 shows the result obtained with the 2W amplifier used for the IFL method. The signal on the left is the injected signal and the signal on the right is the magnetron's signal. As it seen, the signals are not locked in frequency. The magnetron's signal was moving in the vicinity of the injected signal without any success in this test. Later on, a 10W amplifier was used to see if the IFL could be achieved with a high-power signal injected instead of the low-power signal previously used. Also, by controlling the magnetron's current, the output power was lowered to 660W. The result was impressive, interaction was observed between the signal injected and the magnetron's signal. Figure 3.8 shows this interaction.

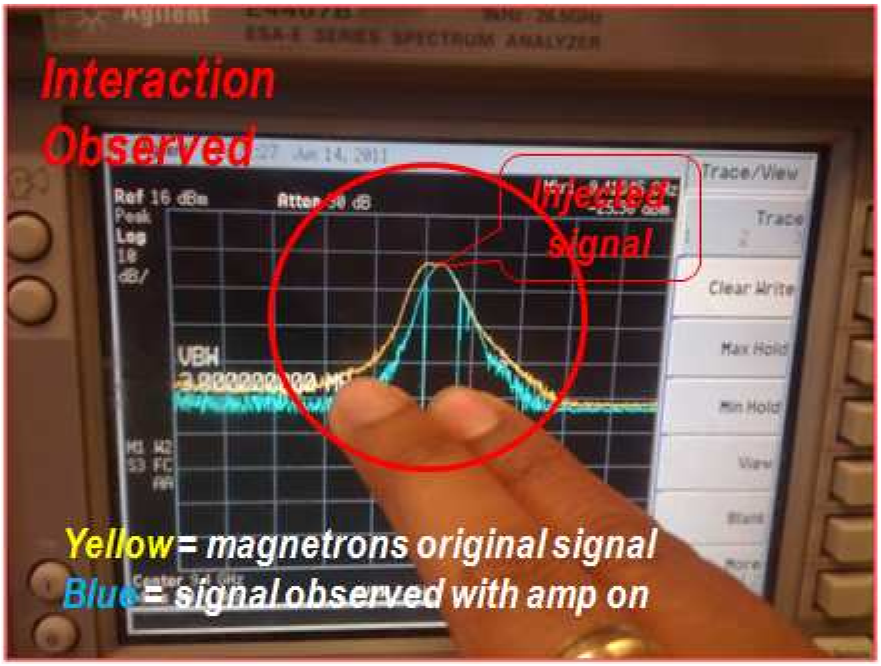

Figure 3.8 Interaction between injected signal and magnetron's signal

Even though the magnetron's power was lowered considerably, the previous picture shows that the method works. Another test was conducted to examine whether the magnetron could be frequency-unlocked with temperature once it was locked by injecting the signal. It is of common knowledge that a circuit or a component within a circuit experience changes in its properties depending on the temperature. The magnetron is not the exception. Table 3.3 shows how the magnetron's temperature changes as it heats up over time.

Table 3.3 Magnetron's temperature change over time

Time (minutes)	Temperature °C
0	26.5
5	31
10	32
15	32.5
20	32.8
25	33.1
30	33

Likewise, figure 3.9 graphically represents the data on table 3.3. It was observed that the magnetron reached a steady temperature of 33°C after 30 minutes passed.

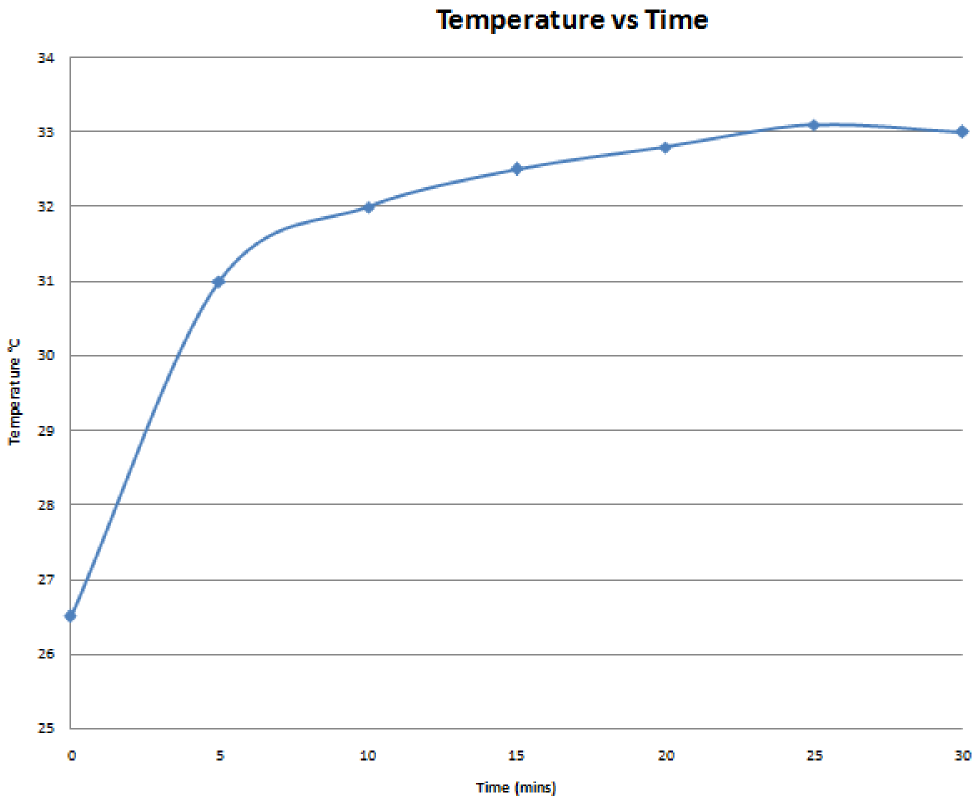

Figure 3.9 Magnetron's Temperature vs. Time

A piezo-electric was used to cool down the magnetron below its natural temperature and a heat gun was used to heat it up above its natural temperature. The frequency and the temperature were observed during this test and the data collected was organized in table 3.4.

Table 3.4 Observed Magnetron’s Frequency Dependence on Temperature

Temperature °C	frequency (GHz)
23	9.406
24	9.40575
25	9.4055
26	9.40525
27	9.40525
28	9.405
29	9.40475
30	9.4045
31	9.404
32	9.403857
33	9.40375

34	9.4035
35	9.40325
36	9.403
37	9.40275
38	9.4025

The plotted data from Table 3.4 is presented in Figure 3.10.

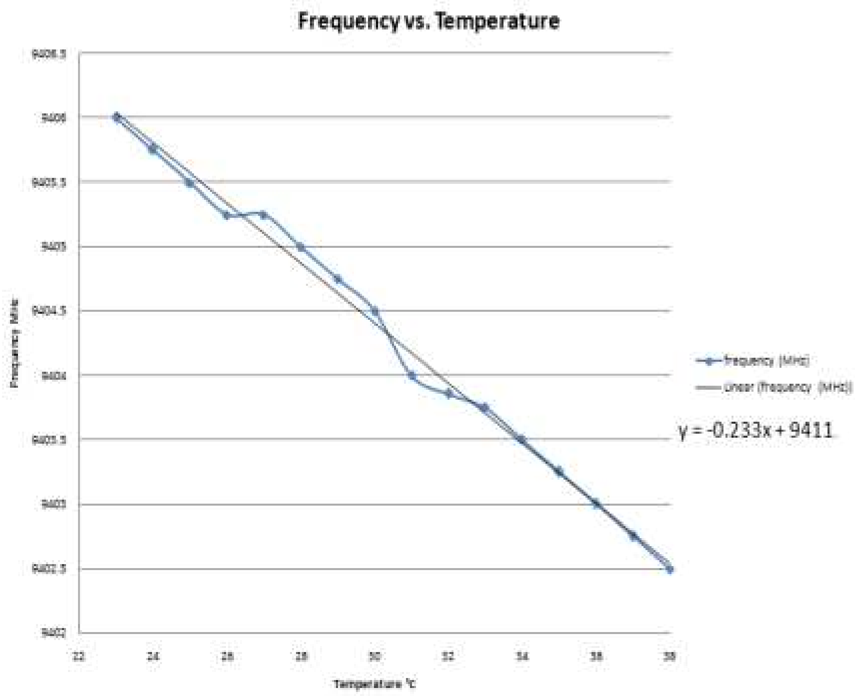

Figure 3.10 Magnetron's frequency changes due to temperature

The error in velocity of a Doppler radar taking into account this frequency drift was calculated using equation 2.13. From the graph in figure 3.10 it is known that the frequency drifts 3.5 MHz in a 15°C interval which results in 0.037% of error in velocity calculations.

Knowing this temperature dependency of circuits and knowing that the IFL was achieved with the magnetron transmitting at 660W the temperature test was performed again while the magnetron was locked in frequency with the injected signal. The heat gun was used and Figure 3.9 shows the effect of heating the magnetron with a heat gun.

Figure 3.11 Frequency drift when heating the magnetron

The frequency of the magnetron drifted as the temperature was changed meaning that the frequency was unlocked. Revising literature again, it was found that to achieve a successful frequency lock the power of the signal injected should be 2% of the transmitted signal's power [*Tahir, 2006*]. For 660 W, 2% is 13.2 W and a 10 W amplifier was used. The interaction was seen because the injected signal was close to the 2% of the transmitted signal; but 10 W weren't enough to keep the magnetron's frequency locked.

To lock a 4kW magnetron, 80 W are needed (2% of 4,000 W). The only 80 W amplifier found, a LM12CL from National Semiconductors, is obsolete and since the price of the 10 W amplifier is around $10,000, an 80 W amplifier will raised the project's cost dramatically. This approach, even though it is possible, it is not recommendable if the cost needs to be low.

4. Pseudo Coherent Method

4.1 Method Explained

The pseudo-coherent method consists of having the transmitted signal as a reference and compared it with the received signal from weather echoes. This signal comparison is further processed to retrieve Doppler measurements. Figure 4.1 presents the circuit implemented for the pseudo coherent method. This circuit was integrated in the radar as separate components; but a single board schematic can be done to have all the components integrated. All the components are placed in the receiver path, after the front end receiver as shown in figure 4.1. The echo is received at 9.41 GHz and the front end receiver down converts this signal to the IF frequency of 60 MHz. Then, this signal passes through the logarithmic amplifier detector which generates three outputs. One output is used to get the reflectivity measurement and the other two were sent to the I/Q demodulator. Once the signal is in the demodulator, it gets divided in the I and Q components of the received echo wave and sent into the DAQ card for processing. A 10 MHz signal crystal oscillator was used as the clock for the DAQ card and as the LO input to the I/Q demodulator, a 120 MHz signal. In addition, the multiplier's output signal of 120 MHz was used as the reference signal in the phase lock loop (PLL) and the PLL is used to stabilize the VCO's frequency drift.

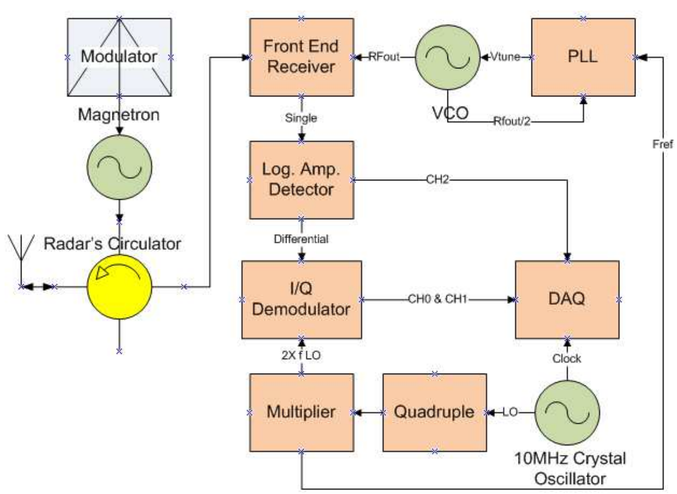

Figure 4.1 Pseudo Coherent Schematic

4.2 Materials

The following devices were used to complete the schematic mentioned in the previous section.

1. FURUNO® radar – Marine radar used by CASA to monitor weather events.
2. Front-End Receiver – The receiver converts the receive signal to an IF signal. The receiver used needs an external LO input to down convert the RF signal to IF signal.
3. Signal Generator or VCO –The VCO is used as the LO input for front end receiver.
4. Phase Lock Loop (PLL) – It is used to stabilize the VCO. It sends a voltage to the V_{tune} pin for the VCO to adjust the RF output signal.
5. Logarithmic Amplifier Detector – It receives the IF signal and provide three outputs, a single voltage output and two differential outputs. The single output goes to the DAQ card for processing to obtain rain reflectivity measurements.
6. I/Q Demodulator – It receives the differential output from the detector and obtains the I and Q signals of the signal received. These signals are sent to the DAQ card for processing to obtain velocity measurements.
7. DAQ card – A four-channel data acquisition card. It is used to process the data obtained.
8. 10 MHz Crystal Oscillator – Works as the clock for the DAQ card and as the LO for the I/Q demodulator.
9. Multipliers – Multiplies the 10 MHz signal from the crystal oscillator to reach the frequency needed as the LO for the I/Q demodulator and the PLL reference signal.

4.3 Cost

The following table shows the preliminary cost of the parts for the radar unit with these modifications. Also, the table includes the solar power system and the wireless connection equipment cost. This represents the total cost of a complete OTG node in development for the radar network established in the island.

Table 4.1: Pseudo Coherent Radar node Cost as of Fall 2011

Radar Subsystem Parts	Price	
4kW FURUNO Radar	$	7,495.00
Parabolic Antenna w/Manual adjust	$	4,495.00
PCI9816H/512 DAQ card	$	1,910.00
Computer Hardware and Software	$	300.90
Sub total 1	**$**	**14,200.90**
Wireless Connection	**Price**	
ODU External (RDW-WL 1000) (2)	$	1,153.40
IDU-E (radio/module) (2)	$	624.10
Antennas (24dBi, parabolic grid) (2)	$	108.76
LMR-400 (cables) (2)	$	33.38
Data/Signal Surge Protector (2)	$	154.98
Lightning Arrestor (2)	$	79.06
CAT5, 50M, RJ45 conn. (LAN cable)	$	188.02
D-Link Switch (4 ports)	$	40.82
Web Power Switch	$	113.95
Sub total 2	**$**	**2,496.47**
Miscellaneous	**$**	**500.00**

Radar Parts for Doppler capabilities	Price	
Demodulating Log. Amp Detector	$	100.19
I/Q Demodulator	$	125.00
30 dB Attenuator (2)	$	23.90
20 dB Attenuator	$	11.95
NJT1946A Front End Receiver	$	365.00
Crystal Oscillator	$	260.00
Low Noise HF Quadrupler	$	312.00
Low Noise Odd Order Multiplier	$	591.00
VCO Evaluation Board	$	397.00
Phase Lock Loop Evaluation Board	$	551.00
Sub total 3	**$**	**2,737.04**
Solar Power Sub-System	**Price**	
Solar Panels (2)	$	800.00
Batteries (2)	$	450.00
Solar Charger	$	200.00
Power Inverter	$	200.00
Sub total 4	**$**	**1,650.00**
grand total	**$**	**21,584.41**

4.4 Process

Once the devices and materials were received, they were individually characterized to know their behavior and performance. Some of the components were not received on time and all of them depend of an input voltage to control their performance. The characterization of the components received showed the correct tune-voltage in order to obtain the best performance of the circuits. After the characterization, the components received were connected together in the FURUNO® marine radar unit and a test was conducted. This test showed how the components received work with the radar unit and the results will be shown in this section.

4.4.1 Front-end receiver characterization

The front end receiver of the radar was replaced with the NJT1033 front end receiver. The NJT1033 was borrowed from the Microwave Remote Sensing Laboratory (MIRSL) at the University of

Massachusetts and provided by New JRC a company that produces various RF components. This front end receiver was used because it was custom made to input an external LO signal. Figure 4.2 depicts the low noise front end receiver (LNFE).

Figure 4.2 Front end receiver

The external LO signal can be controlled and this allows a more stable receive signal. The LNFE receiver was powered with a 5V voltage. A signal at 9.342 GHz was produces using the VCO powered with 5V and using a tuning voltage (V_{tune}) of 4.9V. Another signal was created with a signal generator and inputted in the LNFE to simulate a received signal. This signal was at 9.402 GHz with a power of -30 dBm. Figure 4.3 shows the signal observed with this test. The output of the LNFE receiver was seen at 60 MHz with a power of -33 dBm.

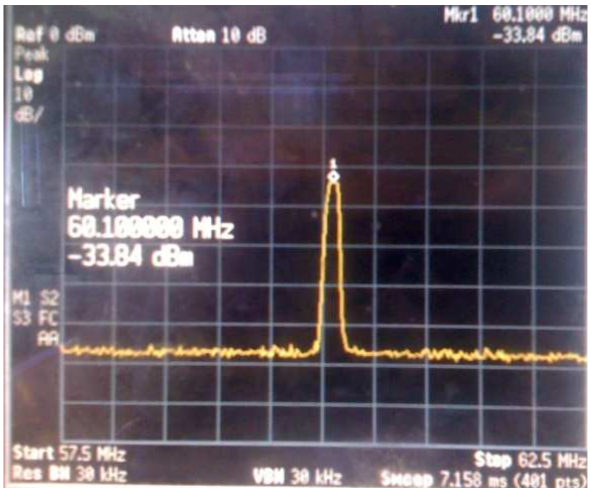

Figure 4.3 LFFE receiver output

4.4.2 Logarithmic amplifier detector characterization

The logarithmic amplifier detector was characterized as well. A supply voltage of 7V was used to power the circuit on and a 60 MHz signal was generated with a signal generator and inputted to the detector. Figure 4.4 shows the board of the logarithmic amplifier used to achieve the objectives.

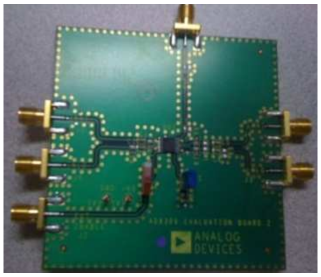

Figure 4.4 Logarithmic amplifier detector

A power sweep was done in the inputted signal from -110 to 20 dBm. This sweep allowed to obtain voltage readings in the V_{log} output of the detector that showed the behavior of the detector as the power of the inputted signal increased. The data obtained is shown in table 4.2.

Table 4.2 Logarithmic amplifier characterization data

Input Power (dBm)	Output Voltage (V)
-110	0.344
-105	0.344
-100	0.346
-95	0.354
-90	0.35
-85	0.352
-80	0.499
-75	0.6
-70	0.501
-65	0.601
-60	0.698
-55	0.801
-50	1.102
-45	1.201
-40	1.102
-35	1.201
-30	1.299
-25	1.399

-20	1.697
-15	1.801
-10	1.699
-5	1.803
0	1.902
5	2.002
10	2.106
15	2.222
20	2.252

Figure 4.5 shows the data obtained plotted. As expected, the output voltage increased as the input power increase; but there were some data points unexpected were the voltage decreased.

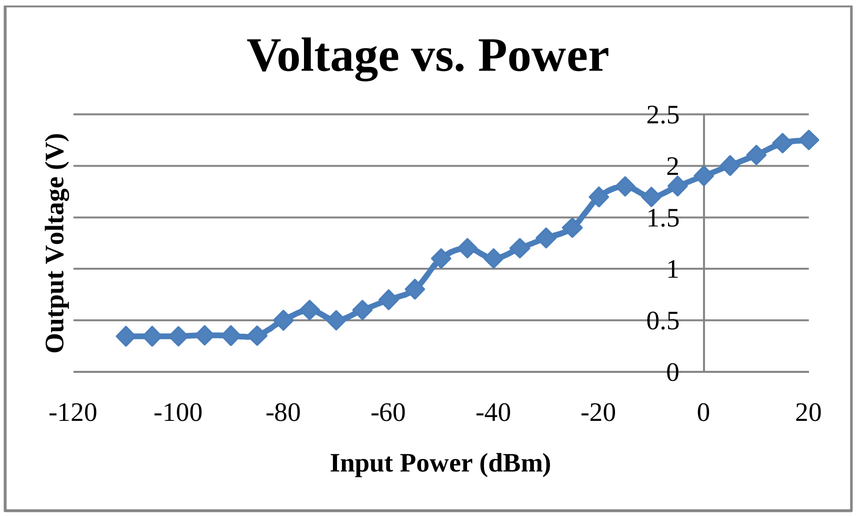

Figure 4.5 Logarithmic amplifier output voltage

The other two outputs of the detector were observed with an oscilloscope and a sine wave signals was always observed. Figure 4.6 shows these sine waves observed with the oscilloscope. These sine waves were 180 degrees apart from one another.

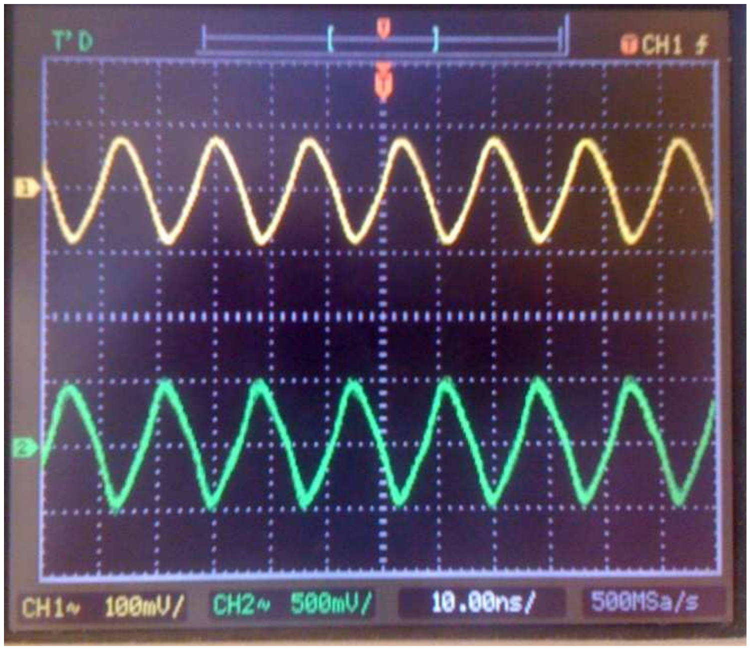

Figure 4.6 Logarithmic amplifier differential output

4.4.3 Demodulator characterization

The demodulator shown in figure 4.7 was used to achieve our objectives. It was characterized as well. This evaluation board has various pins that need a voltage for the circuit to operate. V_{cc1} and V_{cc2} pins need 3V, V_{cc3} needs 5V and V_{ctrl} needs 0.6V.

Figure 4.7 Demodulator evaluation board

In addition, a 60 MHz signal with a power of -40dBm was created with a signal generator and FM modulated at 1KHz. This signal simulated the detector's output and was used as the inputted signal to the demodulator. Another signal was created as well; but this signal was used as the LO for the demodulator. This signal, according to the data sheet, is twice the LO signal. In order to characterize the circuit, a signal of -3dBm at 130 MHz was used. The resulted I and Q signals outputs are shown in Figure 4.8. It can be seen from the figure that these signals are 90 degrees apart with a frequency of 10 MHz as expected.

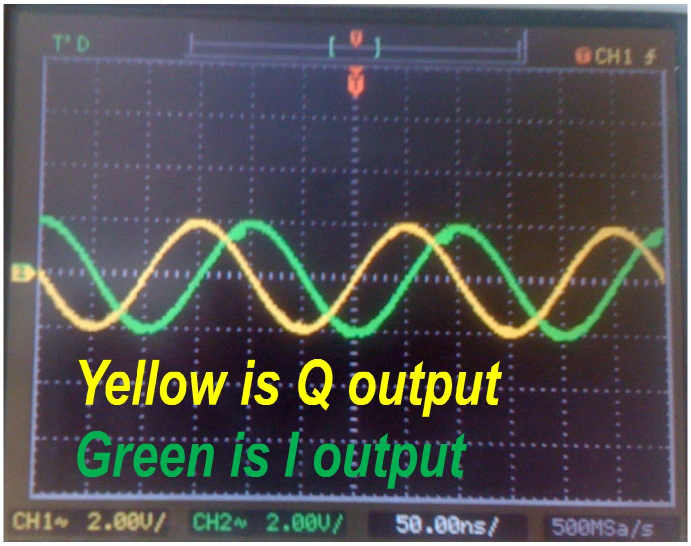

Figure 4.8 Demodulator's output

To implement the pseudo-coherent method the demodulator's output signals are needed at baseband before going into the DAQ card. This is to set up the DAQ card at 1V or 5V according to our needs. Changing the LO signal to 120 MHz allowed to have these baseband signals. During the characterization, it was noted that these signals were biased by 2V. In order to maximize the number of bits used by the DAQ card a differential amplifier is going to be used.

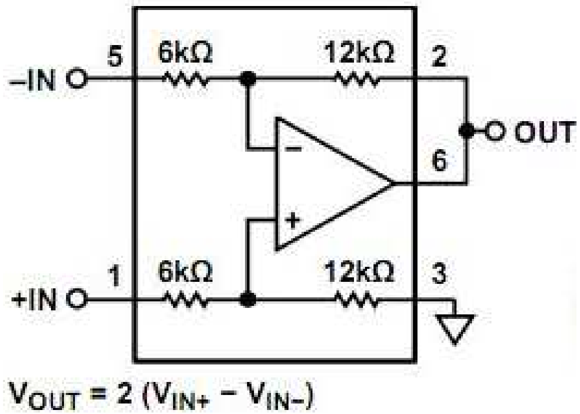

Figure 4.9 Differential amplifier used to eliminate bias

Figure 4.9 shows the circuit that needs to be implemented in the I and Q outputs of the demodulator to eliminate the 2V bias. The voltage reading obtained from the demodulator drift 400mV. The amplifier that will be used has a gain to double this amount (*G=2*) in order to maximize the use of the DAQ card. The DAQ card will observed signals from -800mV to 800mV.

4.4.4 Phase lock loop characterization

The phase lock loop (PLL) was used to stabilize the VCO. This synthesizer has an integrated feedback loop that compares the output signal with a reference signal and adjusts this signal by sending a different tune voltage to the VCO. To characterize this board 5V were used as supply voltage. In addition, the PLL needs basic configuration setup in order to work properly.

The decimal values of counters *A* and *S* in the PLL needed to be found. From the datasheet, these values are defined as:

$$A = int\left(\frac{N}{8}\right) - 1 \tag{4.1}$$

and

$$S = N - 8(A + 1) \tag{4.2}$$

where *N*= 16 to 519. For a valid division ratio *N*, the *A* and *S* counters must satisfied the condition:

A+1≥ S. To calculate N, we look at two different frequencies F_{0_VCO} and F_{ref}. These frequency values in our design are 9360 MHz and 120 MHz, respectively. The ratio among these quantities is taken as our division ratio N.

$$N = \frac{F_{0\_VCO}}{F_{ref}} \tag{4.3}$$

This yield N = 78. With this value of N we calculated the A counter and the S counter. These values are 8 and 6, respectively; values that satisfied the condition mentioned above. Then these values were changed to binary numbers as illustrated in table 4.3.

Table 4.3 Counters values changed into binary numbers

Decimal number	A_5	A_4	A_3	A_2	A_1	A_0 *(LSD)*
A=8	0	0	1	0	0	0
	S_2	S_1	S_0 *(LSD)*			
S=6	1	1	0			

The binary values in the table were generated by using a short circuit to ground for every 0 digit and applying a voltage of 5V to every 1 digit, respectively. The reference signal of 0 dBm and 120 MHz was applied, and the output voltage observed was 4.94 V, resulting in sufficient voltage to be used as the V_{tune} in the VCO.

4.4.5 Tests and Results

A test was conducted to observe the leakage of the magnetron that reached the receiver. To do this, the LNFE receiver was disconnected from its proper place in the radar unit and a 50Ω load was used in place of the antenna. The spectrum analyzer was connected where the receiver goes and the power leakage from the magnetron was measured at this point. Figure 4.10 shows the measurement obtained from the magnetron's leakage signal.

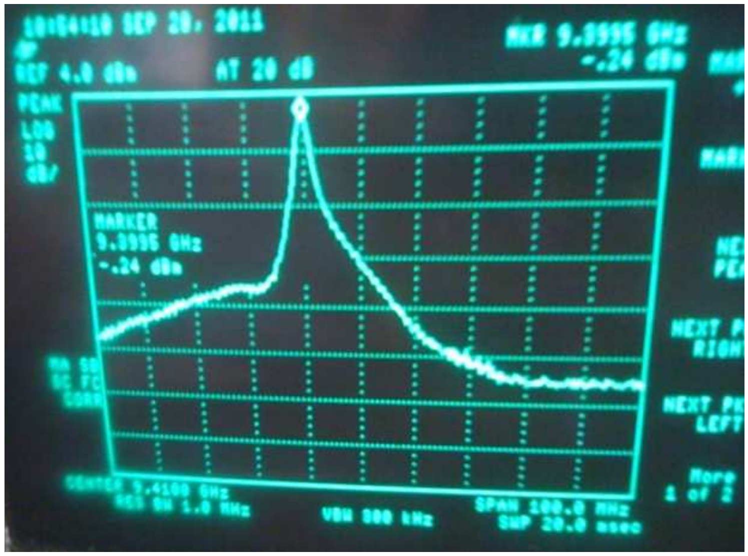

Figure 4.10 Leakage going into the receiver

It can be observed from the previous picture that the power going into the receiver is -0.24 dBm at a frequency of 9.3995 GHz. This amount of power is equal to 0.95 mW and corresponds to the computed leakage power. According to the datasheet of the LNFE receiver this amount of power can be detected by the receiver, as required to achieve our objectives. Thus, a second test was performed to observe the output of the LNFE receiver once this leakage signal is received. Figures 4.11 and 4.12 show the signals obtained with the oscilloscope. The first figure shows a train of pulses, which is characteristic of the magnetron's behavior. The second figure shows a zoom to one of these pulses, a rectangular-like shape can be depicted in the figure. According to the reading in the oscilloscope, the signal has a width of 940 ns even though the square pulse the magnetron sends is suppose to have a width of 800 ns. This difference was caused by the initial peak seen in the figure that is related to the excitation of the magnetron and by the oscilloscope itself that provided the measurement until the pulse's fall-time ended.

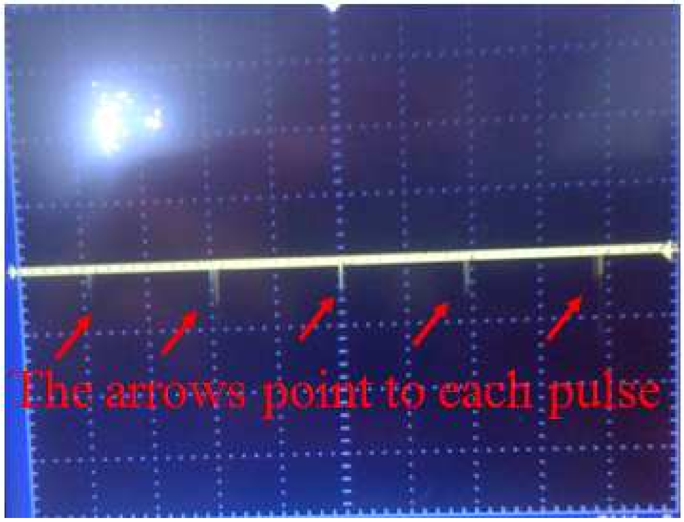

Figure 4.11 Pulse train observed at LNFE's output

Figure 4.12 Zoom view to one of the pulses observed

In addition, a third test was conducted to observe the circuit response when a signal was injected in the circulator simulating a received echo from the atmosphere. The RF echo simulated signal had a power of -30 dBm at a frequency of 9.402 GHz. This signal was created with a microwave signal generator and pulse modulated with a period of 1ms and a width of 800 ns.

When the pulsed echo was inputted, the V_{log} output at the logarithmic amplifier board ranged from 0.696 V to 0.802 V. In addition, the I and Q signals obtained at the demodulator's output were 92.6° apart and had a voltage of 2.53 V and 2.54 V, respectively. These voltages are biased by 2V because the differential amplifier to eliminate the bias was not implemented this time. Figure 4.13 shows the signals obtained. The yellow signal is the in-phase signal (I) and the blue one is the quadrature-phase signal (Q). It can be observed that some noise was generated due to the path that the received echo traveled in the circuits.

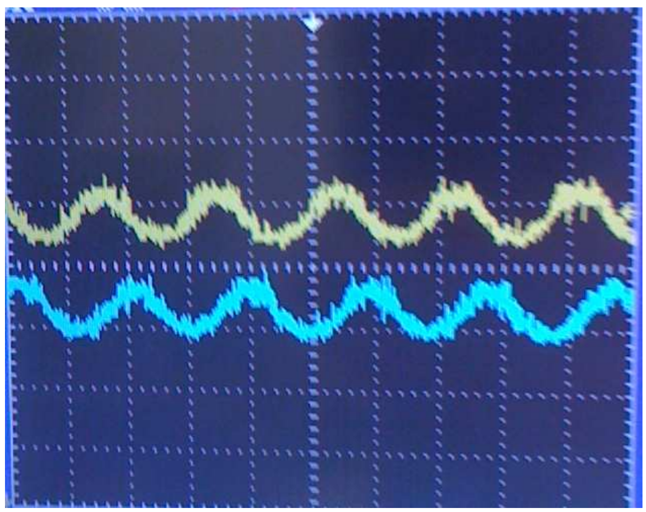

Figure 4.13 I and Q signals obtained simulating a received echo

5. Challenges Solution

5.1 RPM

To acquire accurate Doppler data the antenna of the radar unit should revolve slowly to prevent errors because of the vibration of the radar and to prevent the loss of data for spinning to fast. The CASA OTG radar normally gives 26 revolutions per minute (RPM). To achieve the objectives of this project the antenna should rotate with a speed of 4 to 5 RPM. Two approaches were considered for the design. The first method tries to reduce the revolutions per minute by changing the amount of gears used. Adding more gears can reduce the RPM significantly; but the teeth ratio and the radius of the added gears needed to be computed. Using equations 5.1 and 5.2 let us obtain the relation of transmission which leads to find the velocity of rotation of the motor.

$$i = \frac{N_1}{N_2} \tag{5.1}$$

$$V_2 = iV_1 \tag{5.2}$$

In these equations N_1 and N_2 are the number of teeth of each gear, i is the transmission relation and V_1 and V_2 are the velocity of rotation of the gears. Figure 5.1 shows the motor and teeth ratio of the radar unit.

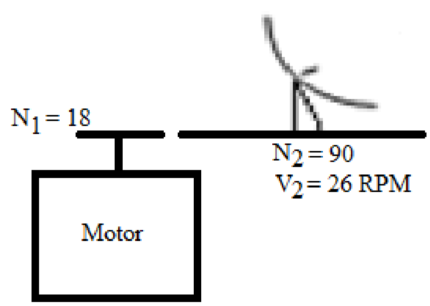

Figure 5.1 Relation among the gears in the radar

Knowing these values the velocity V_1 was computed and resulted in a value of 130 RPM. In addition, assuming a desired rotation speed equal to 4 RPM, the relation of teeth in a multiple gear system was found. Figures 5.2 and 5.3 show how the system looks like changing the gears in the radar and adding two more gears. For this approach to be implemented another housing for the radar unit is needed because the space available in the radar is very limited. In both figures the speed of rotation is shown resulting in V_2 equal to V_3 because both gears are installed in the same axis.

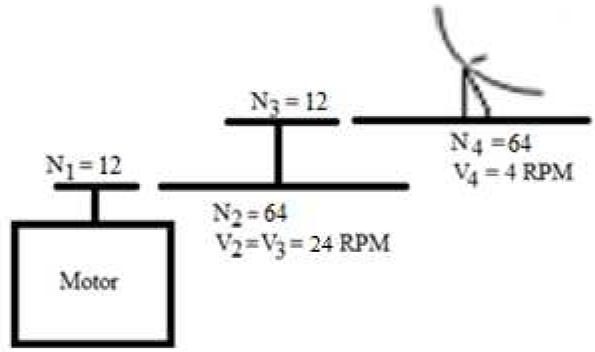

Figure 5.2 System with gears added

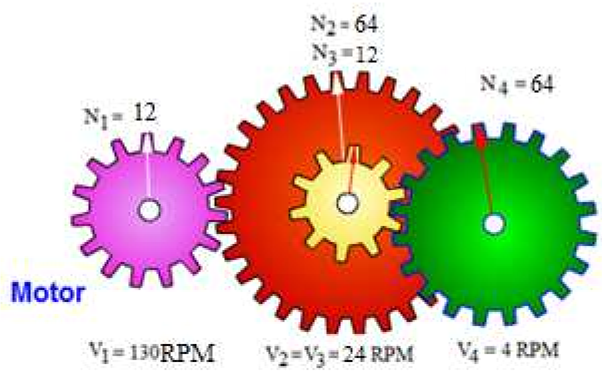

Figure 5.3 Top view of gears (not scaled)

The second approach taken was to contact Electro Marine a marine radar reseller company in Canada. This company is UPRM's marine radar provider and there is a good relationship with them. They have considered a stepper motor system to control the speed of rotation of the antenna. The advantage of using a stepper motor is that the slower they run, the higher the torque. They will have these modifications implemented in the next couple of months to make the system capable of pointing and tracking targets as opposed to historical once-per-scan tracking system.

5.2 Frequency Tuning

Tuning the frequency of the LNFE receiver of the radar unit was an obstacle. The front end receiver of the radar unit did not have any external inputs to control the LO frequency of the receiver. This was very important to have accurate Doppler data estimation. If the frequency drift in the receiver was not stabilized the data obtained would result in errors due to frequency drifts. To solve this issue the LNFE receiver was changed for one provided by New JRC. This new receiver allows the user to input a signal to be used as the LO for the receiver. The signal used in this case came from the VCO, but it was found that it took 30 minutes for the VCO to stabilize in frequency due to the heat produced by the circuit. The heat affected the performance of the VCO resulting in an incorrect IF signal obtained from the LNFE receiver. Figure 5.4 shows how the output frequency of the front end receiver changed depending on the temperature of the VCO. It took 30 minutes for the VCO to stabilize and for the LNFE to have an output frequency of 60 MHz.

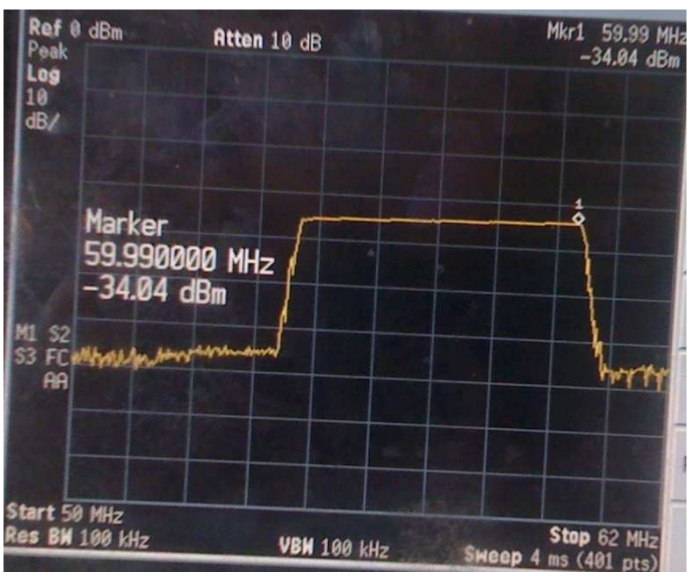

Figure 5.4 Rx frequency drift due to heat in the VCO

To solve this new problem a phase lock loop (PLL) was used. According to the characterization of the PLL, an output voltage of 4.94V was observed. This voltage was applied to the V_{tune} pin on the

VCO and a feedback signal from the VCO's output was injected back to the PLL. The connections made between the PLL and the VCO are shown in Figure 5.5.

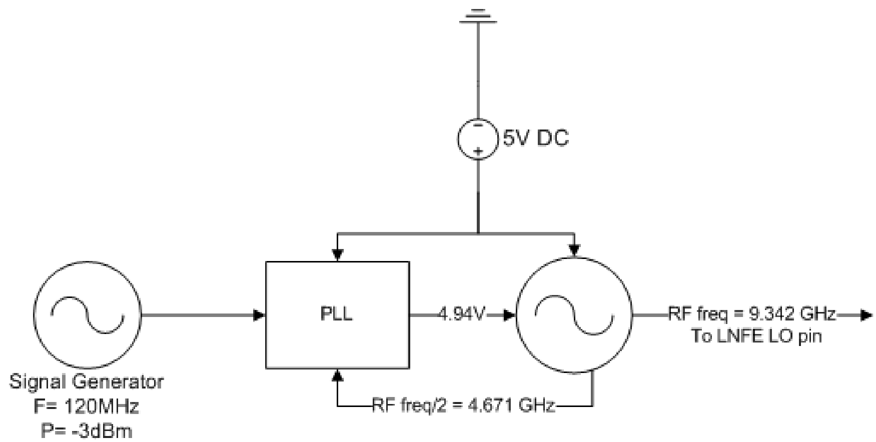

Figure 5.5 Frequency tuning schematic

With this feedback loop implemented the VCO took less than a second to stabilize and the LO frequency used in the LNFE was the output of the VCO. The VCO's output is depicted in figure 5.6. It is shown that the VCO signal is stable at 9.341 GHz with a power of -10.01 dBm. With this stable VCO output the LNFE receiver's output was 60 MHz as shown in figure 5.7 below.

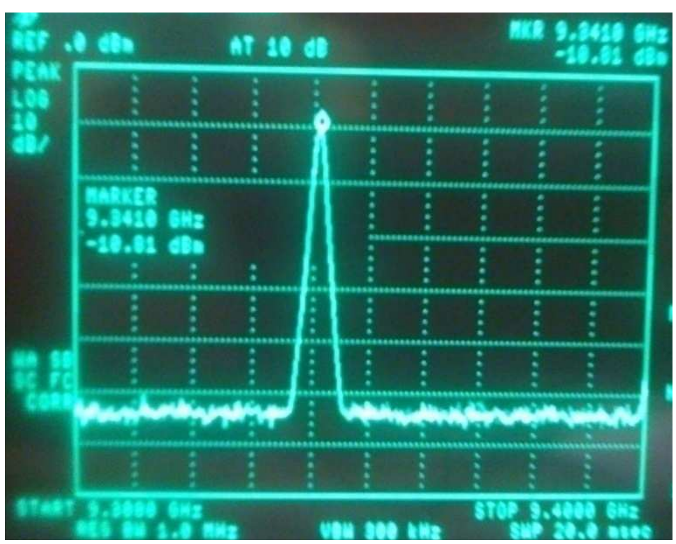

Figure 5.6 VCO's stable output

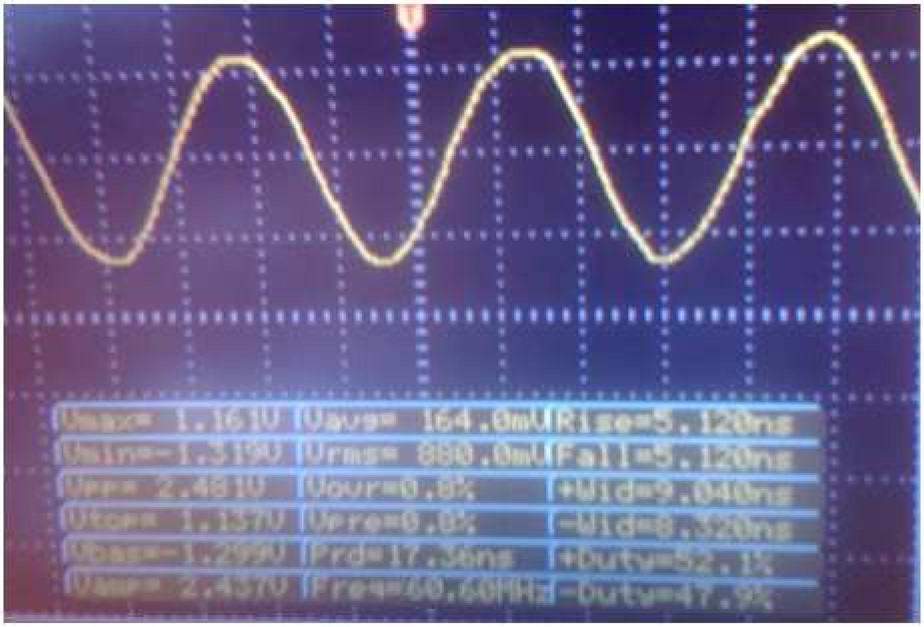

Figure 5.7 LNFE receiver stable output

5.3 Transmitter Pulse Repetition Frequency (PRF)

The PRF of the FURUNO® marine radar is fixed according to the range settings in the processor box. Currently, the PRF is set to 600 Hz for a range of 15.36km. The maximum PRF is 2100 Hz; but this allows visibility up to 2.778km. To solve this problem dual PRF techniques and staggered PRF techniques were considered. Staggered PRF is a transmission process were the listening time from the radar changes slightly. The change of repetition frequency allows the radar to differentiate between returns from its own transmissions and returns from another nearby system with the same PRF and similar radio frequency. With staggered PRF the radar's own targets appear stable in range in relation to the transmitted pulse while echoes from other systems may be uncorrelated, causing them to be rejected by the receiver. The dual PRF technique was introduced in 1976 and consists in having two alternating pulse repetition frequencies [*Holleman et al.*, 2003].

From Equation 2.13 it is clear that the use of different PRF results in different unambiguous velocities. The folding of a measured velocity will, therefore, be different for the two pulse repetition frequencies. By combining the velocity measurements obtained of the two PRF's, the unambiguous velocity interval can be extended. This is done using a high and low PRF combination such that the two unambiguous velocities are related in the following way:

$$\frac{V_h}{V_l} = \frac{PRF_h}{PRF_l} = \frac{N+1}{N} \tag{5.3}$$

where the integer *N* is the dual PRF unfolding factor. The extended unambiguous velocity is given by:

$$V_{lh} = \frac{V_h V_l}{V_h - V_l} \tag{5.4}$$

With typical applications of dual PRF techniques, an unfolding factor *N* of 2, 3 or 4 is used; using higher unfolding factors will result in poor velocity measurements [*Holleman et al.,* 2003]. This technique of dual PRF is going to be implemented with the OTG radar to extend the unambiguous velocity beyond 4.78 m/s. Using a ratio of 3:2, PRFs of 2100 Hz and 1200 Hz, the unambiguous velocity is extended to 22.31 m/s according to equation 5.4. This represents measurements of a 9 in the Beaufort scale that goes up to 12. The Beaufort scale is a measure that relates wind speed to the observed conditions at sea and land; it is normally used in weather forecasts.

5.4 DAQ Programming

To achieve the objectives a program should be written to manage the data received by the DAQ card. Figure 5.8 shows the flow chart of the program that is necessary for the radar to obtain Doppler measurements.

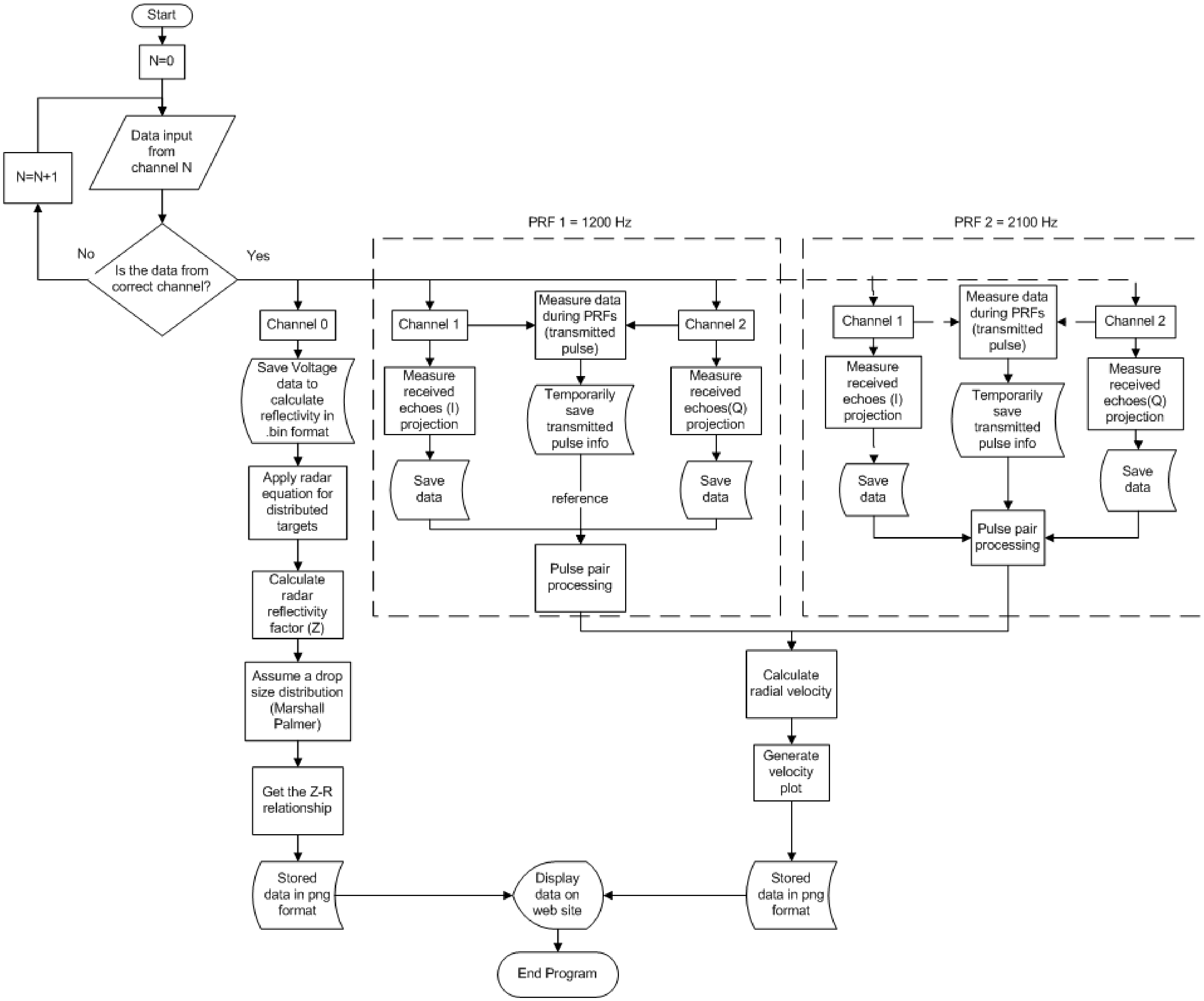

Figure 8 Flow Chart

6. Conclusion and Future Work

6.1 Summary

The first chapter of this project report provided an insight into the motivation to pursue this research. In addition, two main objectives were presented. This chapter also contained a literature review on the ongoing work on weather radars. The second chapter presented in some detail the theory needed to understand this project. Important equations used during the project were described in this chapter as well. In addition, system specifications were mentioned because they were used as reference during the project.

The third chapter presented the proposed IFL method attempted as part of the work in this project report; but not applied due to the increase in the project's cost. Even though this method was not applied the experiments were described and observations were analyzed and discussed. In the fourth chapter, the pseudo coherent method was explained. The experiment's procedures were carefully described and the results were analyzed and presented. It was shown how this method works and how should be implemented.

Chapter five presented the challenges encounter through the project. Most of these challenges were solved and the solutions are presented in the chapter. Finally in chapter six, the research goals are reviewed and the future work is described for the successful implementation of this research.

6.2 Conclusions

This project report has described the development of a low-cost, low-infrastructure marine Doppler radar that will be used for weather applications in the CASA OTG X-Band radar network test bed in Puerto Rico. The results shown in previous chapters demonstrate the successes and accomplishments of this project. All the goals leading to the development of the Doppler weather radar concept were achieved. The major contributions of this research are:

- The injection frequency lock (IFL) study was successfully completed and demonstrated; but not implemented due to the increase of the project's cost.

- The pseudo coherent method was validated and implemented for the most part in the radar unit. The components needed to achieve the desired behavior of the system were found and characterized. Tests were conducted using the circuitry obtained for the method and its functionality was demonstrated. In addition, a simulated RF echo passed through each component and the outputs turned out to be as expected.

- The new gear assembly needed to decrease the RPM of the antenna was designed according to the diameter requirements for the parts already in possession of CASA research group. In addition, communication was establish with Electro Marine, CASA-UPRM's marine radars supplier, for the possibility of having a radar with a stepper motor capable of pointing and tracking targets as opposed to historical once-per-scan tracking system.

- The frequency tuning feedback loop control system was studied and implemented successfully in the radar. This feedback loop between the phase locked loop (PLL) and the voltage controlled oscillator (VCO) helped stabilizing the VCO's output in order to have a stable 60 MHz output in the low noise front end receiver.

- The use of dual PRF transmission to extend the unambiguous Doppler velocity interval was proposed. This is done by alternating the pulse repetition frequencies. A possible combination of the pulse repetition frequencies can be 1200 Hz and 2100 Hz resulting in an extended unambiguous velocity of 22.31 m/s.

- A flow chart was designed to indicate the post processing of the data. This part have not been implemented in the system yet.

- The system was kept low cost with all the modifications. See table 6.1.

Table 6.1 Pseudo Coherent method total cost

Radar Subsystem Parts	Price	
4kW FURUNO Radar	$	7,495.00
Parabolic Antenna w/Manual adjust	$	4,495.00
PCI9816H/512 DAQ card	$	1,910.00
Computer Hardware and Software	$	300.90
Sub total 1	**$**	**14,200.90**
Wireless Connection	**Price**	
ODU External (RDW-WL 1000) (2)	$	1,153.40
IDU-E (radio/module) (2)	$	624.10
Antennas (24dBi, parabolic grid) (2)	$	108.76
LMR-400 (cables) (2)	$	33.38
Data/Signal Surge Protector (2)	$	154.98
Lightning Arrestor (2)	$	79.06
CAT5, 50M, RJ45 conn. (LAN cable)	$	188.02
D-Link Switch (4 ports)	$	40.82
Web Power Switch	$	113.95
Sub total 2	**$**	**2,496.47**
Miscellaneous	**$**	**500.00**

Radar Parts for Doppler capabilities	Price	
Demodulating Log. Amp Detector	$	100.19
I/Q Demodulator	$	125.00
30 dB Attenuator (2)	$	23.90
20 dB Attenuator	$	11.95
NJT1946A Front End Receiver	$	365.00
Crystal Oscillator	$	260.00
Low Noise HF Quadrupler	$	312.00
Low Noise Odd Order Multiplier	$	591.00
VCO Evaluation Board	$	397.00
Phase Lock Loop Evaluation Board	$	551.00
Sub total 3	**$**	**2,737.04**
Solar Power Sub-System	**Price**	
Solar Panels (2)	$	800.00
Batteries (2)	$	450.00
Solar Charger	$	200.00
Power Inverter	$	200.00
Sub total 4	**$**	**1,650.00**
grand total	**$**	**21,584.41**

6.3 Future Work

Once all the parts arrive, they need to be characterized to know their behavior and control their performance. The parts need to be implemented in the system with the rest of the circuits. A post processing program needs to be developed following the flow chart presented in chapter 5. This program should be able to help the user understand and use the data captured. An FPGA (Field-Programmable Gate Array) Card can be used to generate the dual PRF signals with the desire pulse length and timing control. Calibration and verification of the pseudo coherent method implementation and Doppler velocity estimates can be achieved from data comparison with other Doppler radars in Puerto Rico, the TropiNet X-band radar network. This can be performed once the parts needed are received and implemented on the system. In addition, a voltage regulator could be used to power the circuits added in the system. X-band frequency provides higher resolution, but attenuation limits the precision of rainfall estimates. Studies on attenuation in tropical areas could improve estimates at long range. Finally, and more important, integrating the OTG X-band Doppler radar to the radar network already established by CASA research group in Puerto Rico will help in providing coverage gaps in the lower atmosphere were most weather phenomena that affects citizens live occurs.

REFERENCES

Acosta, M. “Clutter Elimination Methods and Data Merging for X Band Weather Radar Network in Complex Terrains”, *MS Thesis*, University of Puerto Rico at Mayagüez, July 2011.

Bharadwaj, Nitin, V. Chandrasekar, F. Junyent, “Signal Processing System for the CASA Integrated Project I Radars”, *J. Atmos. Oceanic Technol.*, 27, 1440–1460, 2010.

Brown, R. and V. Wood, “A Guide for Interpreting Doppler Velocity Patterns: Northern Hemisphere Edition” 2nd ed., NOAA/National Severe Storms Laboratory, Norman, Oklahoma, June 2007.

Cheney, M., Tesla: Man out of time. New York, NY. Touchstone, 1981.

DeVito, P., M. H. Seavey, “Some properties of an injection-locked pulsed magnetron in a coherent-echo-detection system,” *Electronics Letters*, vol. 3, 1967, p. 375-377.

DeVito, P., W. Kearns, and M. Seavey, “Phase Pattern Control of Injection-Locked Pulsed Magnetrons,” *www. cockcroft. ac. uk/public/workshop-jul04/tahir.*, Vol. 24, 1969, pp. 1436-1437.

Holleman, I., H. Beekhuis, “Analysis and correction of dual PRF velocity data”. *J. Atmos. Oceanic Technol.*, **20**, 443–453, 2003.

Joe, P., D. Hudak, C. Crozier, J. Scott, M. Falla, “Signal Processign and Digital IF on the Canadian Doppler Radar Network”. Advanced Weather Radar System seminar, 1998.

Jorgensen, D., T. Shepherd, A. Goldstein, “A dual-pulse repetition frequency scheme for mitigating velocity ambiguities of the NOAA P-3 airborne Doppler radar”. *J. Atmos. Oceanic Technol.*, **17**, 585–594, 2000.

Junyent, F., “NetworkedWeather Radar System using Coherent on Receive Technology”, *PhD. Disertation*, 2007.

McLaughlin, *et al.*, “Short-wavelength technology and the potential for distributed networks of small radar systems,” *Bull. Am. Met. Soc.*, vol 90, pp. 1797-1817, Dec. 2009.

National Instruments, “What is I/Q Data?” Tutorial, April 5, 2011. http://zone.ni.com/devzone/cda/tut/p/id/4805.

Pablos, G., “Off the Grid X-Band Radar Node Development”, *MS Thesis*, University of Puerto Rico at Mayagüez, June 2010.

Richards, M., J. Scheer and W. Holm, Principles of Modern Radars, Vol.1. Raleigh, NC. SciTech Publishing, 2010.

Rinehart, R., Radar for Meteorologists, 5th ed. Nevada, MO. Rinehart Publishing, 2010.

Rodríguez, C., “Calibration and Validation of the First Node of the Meteorological X-Band Radar Network for the West Coast of Puerto Rico”, *M.S. Thesis*, University of Puerto Rico at Mayagüez, May 2009.

Skolnik, M. I., Introduction to Radar Systems, 3rd ed. New York, NY. McGraw-Hill, 1980.

Tahir, I., “Phase and Frequency Locking of Magnetrons by Pushing and Pulling”, *Electron Devices, IEEE Transactions on* , vol.53, no.7, pp.1721-1729, July 2006.

Trabal, J. M., J. Colom-Ustáriz, G. Pablos-Vega, J. Ortiz, W. Castellanos, S. Cruz-Pol, L. León, and R. Rodríguez-Solis, “Low Cost and Minimal Infrastructure Off-The-Grid X- Band Radar Network Development for the West Coast of Puerto Rico”, 2011.

Trabal, J., "Off the Grid Weather Radar Network for Precipitation Monitoring in Western Puerto Rico", ILO Consultant Visit, University of Massachusetts Amherst, April 2011.

Trabal, J., "Puerto Rico Deployable Radar Network Design; Site Survey and Radar Design", *MS Thesis*, University of Puerto Rico at Mayagüez, 2003.

Trabal, J., W. Castellano and J. Ortiz, "Student Test Bed Project: Off the Grid Weather Radar Network for Precipitation Monitoring in Western Puerto Rico", CASA Y8 Site visit presentation, 2011.

Wolff, C., (1997). "Concept of coherence" [Online]. Available: http://www.radartutorial.eu/11.coherent/co05.en.html

Yanauchi, H., O. Suzuki, "Range extension of Doppler radar by combined use of low-PRF and phase diversity processed dual-PRF observations". 33rd International Conference on Radar Meteorology, Australia, 2007.

APPENDIX

APPENDIX A: Components Datasheet List

[1] http://cds.linear.com/docs/Datasheet/5506fa.pdf

[2] http://www.adlinktech.com/PD/marketing/Datasheet/PCI-9816+9826+9846/PCI-9816+9826+9846_Datasheet_1.pdf

[3] http://www.analog.com/static/imported-files/data_sheets/AD8309.pdf

[4] http://www.hittite.com/content/documents/data_sheet/hmc511lp5.pdf

[5] http://www.hittite.com/content/documents/data_sheet/hmc591lp5.pdf

[6] http://www.minicircuits.com/pdfs/VAT-20+.pdf

[7] http://www.minicircuits.com/pdfs/VAT-30+.pdf

[8] http://www.national.com/opf/LM/LM12CL.html#Overview

[9] http://www.rell.com/Pages/Product-Details.aspx?productId=7290

[10] http://www.wenzel.com/pdffiles1/Multipliers/LNHQ.pdf

[11] http://www.wenzel.com/pdffiles1/Multipliers/LNOM.pdf

[12] http://www.wenzel.com/pdffiles1/Oscillators/Instock/501-04608a.pdf